

Quasi-consistent efficient meshfree thin shell formulation with naturally stabilized enforced essential boundary conditions

Junchao Wu^{a,*}, Yangtao Xu^a, Bin Xu^a, Syed Humayun Basha^a

^a*Key Laboratory for Intelligent Infrastructure and Monitoring of Fujian Province, Key Laboratory for Structural Engineering and Disaster Prevention of Fujian Province, College of Civil Engineering, Huaqiao University, Xiamen, Fujian, 361021, China*

Abstract

This research proposed an efficient and quasi-consistent meshfree thin shell formulation with naturally stabilized enforcement of essential boundary conditions. Within the framework of the Hu-Washizu variational principle, a mixed formulation of displacements, strains and stresses is employed in this approach, where the displacements are discretized using meshfree shape functions, and the strains and stresses are expressed using smoothed gradients and covariant bases. The smoothed gradients satisfy the first second-order integration constraint and observed variational consistency for polynomial strains and stresses. Owing to Hu-Washizu variational principle, the essential boundary conditions automatically arise in its weak form. As a result, the suggested technique's enforcement of essential boundary conditions resembles that of the traditional Nitsche's method. Contrary to Nitsche's method, the costly higher order derivatives of conventional meshfree shape functions are replaced by the smoothed gradients with fast computation, which improve the efficiency. Meanwhile, the proposed formulation features a naturally stabilized term without adding any artificial stabilization factors, which eliminates the application of penalty method as a stabilization. Further, the efficacy of the proposed Hu-Washizu meshfree thin shell formulation is illustrated by a set of classical standard thin shell problems.

Keywords: Meshfree, Thin shell, Hu-Washizu variational principle,
Reproducing kernel gradient smoothing, Essential boundary condition

*Corresponding author
Email address: jcwu@hqu.edu.cn (Junchao Wu)

1. Introduction

Thin shell structures generally adhere to the Kirchhoff hypothesis [1], that neglects the shear deformation can be described using Galerkin formulation which requires to have at least C^1 continuity. ~~The traditional~~ Traditional finite element methods ~~usually have typically employ~~ C^0 continuous shape functions, and it prefers ~~Mindlin thick shear theory~~, hybrid and mixed ~~models in simulation of shell structure~~ [3]. ~~Meshfree methods~~ [19, 20, 12] shell models, like linear and nonlinear Mindlin model [2, 3] and the one inextensible director model [4]. Over the past thirty years, various novel formulations with high order smoothed shape functions have ~~garnered much research attention over the past thirty years~~. ~~These techniques been applied to thin shell formulations~~. These include element-free Galerkin method [5], maximum-entropy meshfree method [6], Hermite reproducing kernel particle method [7], peridynamics [8], isogeometric analysis [9], and others. For a more comprehensive review of advances and applications of high order formulations in various scientific and engineering fields, refer to [10, 12, 13, 14, 15, 16, 17, 18]. Among these approaches, Galerkin meshfree methods with moving least square approximation (MLS) [19] or reproducing kernel approximation (RK) [20] established the shape functions based on a collection of dispersed nodes, and high order continuity of shape functions can be easily achieved even with low-order basis functions. For thin shell analysis, high order meshfree approximation can also ~~furhter further~~ alleviate the membrane locking caused by the mismatched approximation order of membrane strain and bending strain [5]. Moreover, ~~nodal-based meshfree~~ node-based MLS/RK approximations generally offer the flexibility of local refinement and can relieve the burden of mesh distortion. ~~Owing to these benefits, numerous meshfree techniques have been developed and implemented in many scientific and engineering fields~~ [10, 11, 6, 15, 14, 16, 17]. However, the high order smoothed meshfree shape functions accompany the enlarged and overlapping supports, which may potentially cause many problems for shape functions. One of the issues is the loss of the Kronecker delta property, which means that, unlike the finite element methods, the necessary boundary conditions cannot be directly enforced [21]. Another issue is that the variational consistency or said integration constraint, which is a condition that requires the formulation to exactly reproduce the solution spanned by the basis functions, cannot be satisfied. This issue is mainly caused by the misalignment between the numerical integration domains and supports of shape functions. Thus, the shape functions exhibit a piecewise nature in each integration domain. Besides, it has to be noted that the traditional integration rules like Gauss scheme cannot ensure the integration accuracy in Galerkin weak form [22, 23]. Therefore, variational consistency is vital to the solution accuracy in the Galerkin meshfree formulations.

Various ways have been presented to enforce the necessary boundary for Galerkin meshfree methods directly, including the boundary singular kernel method [24], mixed transformation method [24], and interpolation element-free method [25] for recovering shape functions' Kronecker property. However, these methods were not based on variational setting and cannot guarantee variational

consistency. ~~In the absence of a meshfree node, accuracy enforcement might be poor.~~ The accuracy may be poor at locations away from the sample points. In contrast, enforcing the essential boundary conditions using a variational approach is preferred for Galerkin meshfree methods. The variational consistent Lagrange multiplier approach was initially used to the Galerkin meshfree method by Belytschko et al. [19]. In this method, the extra degrees of freedom are used to determine the discretization of Lagrange multiplier. Ivannikov et al. [26] extended this approach to geometrically nonlinear thin shells. Lu et al. [27] suggested the modified variational essential boundary enforcement approach and expressed the Lagrange multiplier by equivalent ~~tractions~~ traction to eliminate the excess degrees of freedom. However, the coercivity of this approach is not always ensured and potentially reduces the accuracy. Zhu and Atluri [28] pioneered the penalty method for meshfree method, making it a straightforward approach to enforce essential boundary conditions via Galerkin weak form. However, the penalty method lacks variational consistency and requires experimental artificial parameters whose optimal value is hard to determine. Fernández-Méndez and Huerta [21] imposed necessary boundary conditions using Nitsche’s approach in the meshfree formulation. This approach can be seen as a hybrid combination of the modified variational method and the penalty method because the modified variational method generates variational consistency through the use of a consistent term, and the penalty method is used as a stabilized term to recover the coercivity. Skatulla and Sansour [29] extended Nitsche’s thin shell analysis method and proposed an iteration algorithm to determine artificial parameters at each integration point. Additionally, the Nitsche’s method has been successfully applied to maintain the variational consistency between different geometrical or material domains in problems with multiple patches [30] and composite materials [31].

In order to address the issue of numerical integration, a series of consistent integration schemes have been developed for Galerkin meshfree methods. Among these include stabilized conforming nodal integration [32], variational consistent integration [33], quadratic consistent integration [34], reproducing kernel gradient smoothing integration [35], and consistent projection integration [36]. The assumed strain approach establishes the most consistent integration scheme, while the smoothed gradient replaces the costly higher order derivatives of traditional meshfree shape functions and shows a high efficiency. Moreover, to achieve global variational consistency, a consistent essential boundary condition enforcement must be combined with the consistent integration scheme. The combination of consistent integration scheme and Nitsche’s method for treating essential boundary conditions may demonstrate better performance since both the methods can satisfy the coercivity without requiring additional degrees of freedom. Nevertheless, Nitsche’s approach still retains the artificial parameters in the stabilized terms, and it is essential to remain cautious of the costly higher order derivatives, particularly for thin plate and thin shell problems. Recently, Wu et al. [37, 38] proposed an efficient and stabilized essential boundary condition enforcement method based upon the Hellinger-Reissner variational principle, where a mixed formulation in Hellinger-Reissner weak form recasts the

99 reproducing kernel gradient smoothing integration. The terms required for en-
100 forcing essential boundary conditions are identical to the Nitsche’s method, and
101 both have consistent and stabilized terms. However, the stabilized term of this
102 method naturally exists in the Hellinger-Reissner weak form and no longer needs
103 the artificial parameters, even for essential boundary enforcement. Instead all
104 of the higher order derivatives are represented by the smoothed gradients and
105 their derivatives.

106 In this study, an efficient and stabilized variational consistent meshfree
107 method that naturally enforces the essential boundary conditions is developed
108 for thin shell structures. Following the concept of the Hellinger-Reissner prin-
109 ciple base consistent meshfree method, the Hu-Washizu variational principle of
110 complementary energy with variables of displacement, strains, and stresses were
111 employed. The displacement is approximated by conventional meshfree shape
112 functions, and the strains and stresses were expressed by smoothed gradients
113 with covariant bases. It is important to note that although the first second-order
114 integration requirements were naturally embedded in the smoothed gradients,
115 their fulfillment resulted in a quasi-satisfaction of variational consistency. This
116 is mainly because of the non-polynomial nature of the stresses. Hu-Washizu’s
117 weak form was used to evaluate all the essential boundary conditions regard-
118 ing displacements and rotations. This type of formulation is similar to the
119 Nitsche’s method but does not require any artificial parameters. Compared
120 with Nitsche’s method, conventional reproducing smoothed gradients and its
121 direct derivatives replace the costly higher order derivatives. By utilizing the
122 advantages of a replicating kernel gradient smoothing framework, the smoothed
123 gradients showed better performance compared to conventional derivatives of
124 shape functions, hence increasing the meshfree formulation’s computational ef-
125 ficiency.

126 The remainder of this research article is structured as follows: The kinemat-
127 ics of the thin shell structure and the weak form of the associated Hu-Washizu
128 principle are briefly described in Section 2. The mixed formulation regarding
129 the displacements, strains and stresses in accordance with Hu-Washizu weak
130 form are presented in Section 3. The discrete equilibrium equations are derived
131 in Section 4 using the naturally occurring accommodation of essential. Subse-
132 quently, they are compared to the equations obtained using Nitsche’s method.
133 The numerical results in Section 5 validate the efficacy of the proposed Hu-
134 Washizu meshfree thin shell formulation. Lastly, the concluding remarks are
135 presented in Section 6.

2. Hu-Washizu's formulation of complementary energy for thin shell

2.1. Kinematics for thin shell

Consider the configuration of a shell $\bar{\Omega}$, as shown in Fig. 1, which can be easily described by a parametric curvilinear coordinate system $\boldsymbol{\xi} = \{\xi^i\}_{i=1,2,3}$. The mid-surface of the shell denoted by Ω is specified by the in-plane coordinates $\boldsymbol{\xi} = \{\xi^\alpha\}_{\alpha=1,2}$, as the thickness direction of shell is by ξ^3 , $-\frac{h}{2} \leq \xi^3 \leq \frac{h}{2}$, h is the thickness of shell. In this work, Latin indices take the values from 1 to 3, and Greek indices are evaluated by 1 or 2. For the Kirchhoff hypothesis [5], the position $\mathbf{x} \in \bar{\Omega}$ is defined by linear functions with respect to ξ^3 :

$$\mathbf{x}(\xi^1, \xi^2, \xi^3) = \mathbf{r}(\xi^1, \xi^2) + \xi^3 \mathbf{a}_3(\xi^1, \xi^2) \quad (1)$$

in which \mathbf{r} means the position on the mid-surface of shell, and \mathbf{a}_3 is correspond-

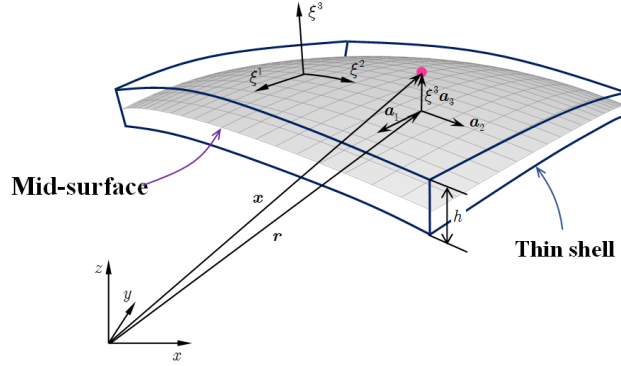


Figure 1: Kinematics for thin shell.

ing normal direction. For the mid-surface of shell, the in-plane covariant base vector with respect to ξ^α can be derived by a trivial partial differentiation to \mathbf{r} :

$$\mathbf{a}_\alpha = \frac{\partial \mathbf{r}}{\partial \xi^\alpha} = \mathbf{r}_{,\alpha}, \alpha = 1, 2 \quad (2)$$

to provide for a clear expression, the subscript comma denotes the partial differentiation operation with respect to in-plane coordinates ξ^α , and the normal vector \mathbf{a}_3 can be obtained by the normalized cross product of \mathbf{a}_α 's as follows:

$$\mathbf{a}_3 = \frac{\mathbf{a}_1 \times \mathbf{a}_2}{\|\mathbf{a}_1 \times \mathbf{a}_2\|} \quad (3)$$

where $\|\bullet\|$ is the Euclidean norm operator.

With the assumption of infinitesimal deformation, the strain components with respect to the global contravariant base can be stated as:

$$\epsilon_{ij} = \frac{1}{2}(\mathbf{x}_{,i} \cdot \mathbf{u}_{,j} + \mathbf{u}_{,i} \cdot \mathbf{x}_{,j}) \quad (4)$$

where \mathbf{u} represents the displacement for the shell deformation. To satisfy the Kirchhoff hypothesis, the displacement is assumed to be of the following form:

$$\mathbf{u}(\xi^1, \xi^2, \xi^3) = \mathbf{v}(\xi^1, \xi^2) + \boldsymbol{\theta}(\xi^1, \xi^2)\xi^3 \quad (5)$$

in which the quadratic and higher order terms are neglected. \mathbf{v} , $\boldsymbol{\theta}$ represent the displacement and rotation in mid-surface, respectively.

Subsequently, plugging Eqs. (1) and (5) into Eq. (4) and neglecting the quadratic terms, the strain components can be rephrased as follows:

$$\begin{aligned} \epsilon_{\alpha\beta} &= \frac{1}{2}(\mathbf{a}_\alpha \cdot \mathbf{v}_{,\beta} + \mathbf{v}_{,\alpha} \cdot \mathbf{a}_\beta) \\ &+ \frac{1}{2}(\mathbf{a}_{3,\alpha} \cdot \mathbf{v}_{,\beta} + \mathbf{v}_{,\alpha} \cdot \mathbf{a}_{3,\beta} + \mathbf{a}_\alpha \cdot \boldsymbol{\theta}_{,\beta} + \boldsymbol{\theta}_{,\alpha} \cdot \mathbf{a}_\beta)\xi^3 \\ &= \varepsilon_{\alpha\beta} + \kappa_{\alpha\beta}\xi^3 \end{aligned} \quad (6a)$$

$$\epsilon_{\alpha 3} = \frac{1}{2}(\mathbf{a}_\alpha \cdot \boldsymbol{\theta} + \mathbf{v}_{,\alpha} \cdot \mathbf{a}_3) + \frac{1}{2}(\mathbf{a}_3 \cdot \boldsymbol{\theta})_{,\alpha}\xi^3 \quad (6b)$$

$$\epsilon_{33} = \mathbf{a}_3 \cdot \boldsymbol{\theta} \quad (6c)$$

where $\varepsilon_{\alpha\beta}$, $\kappa_{\alpha\beta}$ represent membrane and bending strains, respectively, and are given as follows:

$$\varepsilon_{\alpha\beta} = \frac{1}{2}(\mathbf{a}_\alpha \cdot \mathbf{v}_{,\beta} + \mathbf{v}_{,\alpha} \cdot \mathbf{a}_\beta) \quad (7)$$

$$\kappa_{\alpha\beta} = \frac{1}{2}(\mathbf{a}_{3,\alpha} \cdot \mathbf{v}_{,\beta} + \mathbf{v}_{,\alpha} \cdot \mathbf{a}_{3,\beta} + \mathbf{a}_\alpha \cdot \boldsymbol{\theta}_{,\beta} + \boldsymbol{\theta}_{,\alpha} \cdot \mathbf{a}_\beta) \quad (8)$$

In accordance with the Kirchhoff hypothesis, the thickness of shell will not change, and the deformation related with direction of ξ^3 will vanish, i.e. $\epsilon_{3i} = 0$. Thus, the rotation $\boldsymbol{\theta}$ can be rewritten as:

$$\epsilon_{3i} = 0 \Rightarrow \begin{cases} \boldsymbol{\theta} \cdot \mathbf{a}_\alpha = -\mathbf{v}_{,\alpha} \cdot \mathbf{a}_3 \\ \boldsymbol{\theta} \cdot \mathbf{a}_3 = 0 \end{cases} \Rightarrow \boldsymbol{\theta} = -\mathbf{v}_{,\alpha} \cdot \mathbf{a}_3 \mathbf{a}^\alpha \quad (9)$$

where \mathbf{a}^α 's is the in-plane contravariant base vector, $\mathbf{a}^\alpha \cdot \mathbf{a}_\beta = \delta^\alpha_\beta$, δ is the Kronecker delta function. The detailed derivation of Eq. 9 can be found in [39].

Furthermore, on substituting Eq. (9) into Eq. (8) leads to:

$$\kappa_{\alpha\beta} = (\Gamma_{\alpha\beta}^\gamma \mathbf{v}_{,\gamma} - \mathbf{v}_{,\alpha\beta}) \cdot \mathbf{a}_3 = -\mathbf{v}_{,\alpha}|_\beta \cdot \mathbf{a}_3 \quad (10)$$

in which $\Gamma_{\alpha\beta}^\gamma = \mathbf{a}_{\alpha,\beta} \cdot \mathbf{a}^\gamma$ is namely the Christoffel symbol of the second kind, and $\mathbf{v}_{,\alpha}|_\beta$ is the in-plane covariant derivative of $\mathbf{v}_{,\alpha}$, i.e. $\mathbf{v}_{,\alpha}|_\beta = \Gamma_{\alpha\beta}^\gamma \mathbf{v}_{,\gamma} - \mathbf{v}_{,\alpha\beta}$.

2.2. Galerkin weak form for Hu-Washizu principle of complementary energy

In this study, the Hu-Washizu variational principle of complementary energy [40] was adopted for the development of the proposed analytical approach, the

174 corresponding complementary functional, denoted by Π_C , is listed as follows:

$$\begin{aligned}
& \Pi_C(\varepsilon_{\alpha\beta}, \kappa_{\alpha\beta}, N^{\alpha\beta}, M^{\alpha\beta}) \\
&= \int_{\Omega} \frac{h}{2} \varepsilon_{\alpha\beta} C^{\alpha\beta\gamma\eta} \varepsilon_{\gamma\eta} d\Omega + \int_{\Omega} \frac{h^3}{24} \kappa_{\alpha\beta} C^{\alpha\beta\gamma\eta} \kappa_{\gamma\eta} d\Omega \\
&+ \int_{\Omega} \varepsilon_{\alpha\beta} (N^{\alpha\beta} - h C^{\alpha\beta\gamma\eta} \varepsilon_{\gamma\eta}) d\Omega + \int_{\Omega} \kappa_{\alpha\beta} (M^{\alpha\beta} - \frac{h^3}{12} C^{\alpha\beta\gamma\eta} \kappa_{\gamma\eta}) d\Omega \\
&- \int_{\Gamma_v} \mathbf{T} \cdot \bar{\mathbf{v}} d\Gamma + \int_{\Gamma_{\theta}} M_{\mathbf{n}\mathbf{n}} \bar{\theta}_{\mathbf{n}} d\Gamma - (P \mathbf{a}_3 \cdot \bar{\mathbf{v}})_{\mathbf{x} \in C_w}
\end{aligned} \tag{11}$$

175 where $C^{\alpha\beta\gamma\eta}$'s represent the components of fourth order elasticity tensor with
176 respect to the covariant base and plane stress assumption, and it can be ex-
177 pressed by Young's modulus E , Poisson's ratio ν and the in-plane contravariant
178 metric coefficients $a^{\alpha\beta}$'s, $a^{\alpha\beta} = \mathbf{a}^{\alpha} \cdot \mathbf{a}^{\beta}$, as follows:

$$C^{\alpha\beta\gamma\eta} = \frac{E}{2(1+\nu)} (a^{\alpha\gamma} a^{\beta\eta} + a^{\alpha\eta} a^{\beta\gamma} + \frac{2\nu}{1-\nu} a^{\alpha\beta} a^{\gamma\eta}) \tag{12}$$

179 and $N^{\alpha\beta}$, $M^{\alpha\beta}$ represent the components of membrane- and bending- stresses
180 which are given by:

$$N^{\alpha\beta} = h C^{\alpha\beta\gamma\eta} \varepsilon_{\gamma\eta}, \quad M^{\alpha\beta} = \frac{h^3}{12} C^{\alpha\beta\gamma\eta} \kappa_{\gamma\eta} \tag{13}$$

181 Essential boundaries on the edges and corners denoted by Γ_v , Γ_{θ} and C_w
182 are naturally existed in complementary energy functional, and $\bar{\mathbf{v}}$, $\bar{\theta}_{\mathbf{n}}$ are the
183 corresponding prescribed displacement and normal rotation, respectively. \mathbf{T} ,
184 $M_{\mathbf{n}\mathbf{n}}$ and P can be determined by Euler-Lagrange equations of shell problem
185 [39] as follows:

$$\mathbf{T} = \mathbf{T}_N + \mathbf{T}_M \rightarrow \begin{cases} \mathbf{T}_N = \mathbf{a}_{\alpha} N^{\alpha\beta} n_{\beta} \\ \mathbf{T}_M = (\mathbf{a}_3 M^{\alpha\beta} s_{\alpha} n_{\beta})_{,\gamma} s^{\gamma} + (\mathbf{a}_3 M^{\alpha\beta})|_{\beta} n_{\alpha} \end{cases} \tag{14}$$

$$M_{\mathbf{n}\mathbf{n}} = M^{\alpha\beta} n_{\alpha} n_{\beta} \tag{15}$$

$$P = -[[M^{\alpha\beta} s_{\alpha} n_{\beta}]] \tag{16}$$

188 where $\mathbf{n} = n^{\alpha} \mathbf{a}_{\alpha} = n_{\alpha} \mathbf{a}^{\alpha}$ and $\mathbf{s} = s^{\alpha} \mathbf{a}_{\alpha} = s_{\alpha} \mathbf{a}^{\alpha}$ are the outward normal and
189 tangent directions on boundaries. $[[f]]$ is the jump operator defined by:

$$[[f]]_{\mathbf{x}=\mathbf{x}_c} = \lim_{\epsilon \rightarrow \mathbf{0}^+} (f(\mathbf{x}_c + \epsilon) - f(\mathbf{x}_c - \epsilon)), \mathbf{x}_c \in \Gamma \tag{17}$$

190 where f is an arbitrary function on Γ .

191 Moreover, the natural boundary conditions should be applied by Lagrangian
192 multiplier method with displacement \mathbf{v} regarded as multiplier. Thus, then the

new complementary energy functional namely Π is given by:

$$\begin{aligned} & \Pi(\mathbf{v}, \varepsilon_{\alpha\beta}, \kappa_{\alpha\beta}, N^{\alpha\beta}, M^{\alpha\beta}) \\ &= \Pi_C(\varepsilon_{\alpha\beta}, \kappa_{\alpha\beta}, N^{\alpha\beta}, M^{\alpha\beta}) + \int_{\Gamma_M} \theta_{\mathbf{n}}(M_{\mathbf{n}\mathbf{n}} - \bar{M}_{\mathbf{n}\mathbf{n}}) d\Gamma \\ & - \int_{\Gamma_T} \mathbf{v} \cdot (\mathbf{T} - \bar{\mathbf{T}}) d\Gamma - \mathbf{v} \cdot \mathbf{a}_3(P - \bar{P})_{\mathbf{x} \in C_P} - \int_{\Omega} \mathbf{v} \cdot (\mathbf{b} - \bar{\mathbf{b}}) d\Omega \end{aligned} \quad (18)$$

where $\bar{\mathbf{T}}$, $\bar{M}_{\mathbf{n}\mathbf{n}}$ and \bar{P} are the prescribed traction, bending moment and concentrated force on edges Γ_T , Γ_M and corner C_P respectively. All the specified boundaries meet the following geometric relationships:

$$\begin{cases} \Gamma = \Gamma_v \cup \Gamma_T \cup \Gamma_\theta \cup \Gamma_M, & C = C_v \cup C_P, \\ \Gamma_v \cap \Gamma_T = \Gamma_\theta \cap \Gamma_M = C_v \cap C_P = \emptyset \end{cases} \quad (19)$$

and $\bar{\mathbf{b}}$ stands for the prescribed body force in Ω , \mathbf{b} can be written based on Euler-Lagrange equations [39] as:

$$\mathbf{b} = \mathbf{b}_N + \mathbf{b}_M \rightarrow \begin{cases} \mathbf{b}_N = (\mathbf{a}_\alpha N^{\alpha\beta})|_\beta \\ \mathbf{b}_M = (\mathbf{a}_3 M^{\alpha\beta})|_{\alpha\beta} \end{cases} \quad (20)$$

Introducing a standard variational argument to Eq. (18), $\delta\Pi = 0$, and considering the arbitrariness of virtual variables, $\delta\mathbf{v}$, $\delta\varepsilon_{\alpha\beta}$, $\delta\kappa_{\alpha\beta}$, $N^{\alpha\beta}$, $M^{\alpha\beta}$ lead to the following weak form:

$$- \int_{\Omega} h \delta\varepsilon_{\alpha\beta} C^{\alpha\beta\gamma\eta} \varepsilon_{\gamma\eta} d\Omega + \int_{\Omega} \delta\varepsilon_{\alpha\beta} N^{\alpha\beta} d\Omega = 0 \quad (21a)$$

$$- \int_{\Omega} \frac{h^3}{12} \delta\kappa_{\alpha\beta} C^{\alpha\beta\gamma\eta} \kappa_{\gamma\eta} d\Omega + \int_{\Omega} \delta\kappa_{\alpha\beta} M^{\alpha\beta} d\Omega = 0 \quad (21b)$$

$$\begin{aligned} & \int_{\Omega} \delta N^{\alpha\beta} \varepsilon_{\alpha\beta} d\Omega - \int_{\Gamma} \delta \mathbf{T}_N \cdot \mathbf{v} d\Gamma + \int_{\Omega} \delta \mathbf{b}_N \cdot \mathbf{v} d\Omega \\ & + \int_{\Gamma_v} \delta \mathbf{T}_N \cdot \mathbf{v} d\Gamma = \int_{\Gamma_v} \delta \mathbf{T}_N \cdot \bar{\mathbf{v}} d\Gamma \end{aligned} \quad (21c)$$

$$\begin{aligned} & \int_{\Omega} \delta M^{\alpha\beta} \kappa_{\alpha\beta} d\Omega - \int_{\Gamma} \delta M_{\mathbf{n}\mathbf{n}} \theta_{\mathbf{n}} d\Gamma + \int_{\Gamma} \delta \mathbf{T}_M \cdot \mathbf{v} d\Gamma + (\delta P \mathbf{a}_3 \cdot \mathbf{v})_{\mathbf{x} \in C} + \int_{\Omega} \delta \mathbf{b}_M \cdot \mathbf{v} d\Omega \\ & + \int_{\Gamma_\theta} \delta M_{\mathbf{n}\mathbf{n}} \theta_{\mathbf{n}} d\Gamma - \int_{\Gamma_v} \delta \mathbf{T}_M \cdot \mathbf{v} d\Gamma - (\delta P \mathbf{a}_3 \cdot \mathbf{v})_{\mathbf{x} \in C_v} \\ & = \int_{\Gamma_\theta} \delta M_{\mathbf{n}\mathbf{n}} \bar{\theta}_{\mathbf{n}} d\Gamma - \int_{\Gamma_v} \delta \mathbf{T}_M \cdot \bar{\mathbf{v}} d\Gamma - (\delta P \mathbf{a}_3 \cdot \bar{\mathbf{v}})_{\mathbf{x} \in C_v} \end{aligned} \quad (21d)$$

$$\begin{aligned}
& \int_{\Gamma} \delta \theta_{\mathbf{n}} M_{\mathbf{nn}} d\Gamma - \int_{\Gamma} \delta \mathbf{v} \cdot \mathbf{T} d\Gamma - (\delta \mathbf{v} \cdot \mathbf{a}_3 P)_{\mathbf{x} \in C} + \int_{\Omega} \delta \mathbf{v} \cdot \mathbf{b} d\Omega \\
& - \int_{\Gamma_{\theta}} \delta \theta_{\mathbf{n}} M_{\mathbf{nn}} d\Gamma + \int_{\Gamma_v} \delta \mathbf{v} \cdot \mathbf{T} d\Gamma + (\delta \mathbf{v} \cdot \mathbf{a}_3 P)_{\mathbf{x} \in C_v} = - \int_{\Gamma_T} \delta \mathbf{v} \cdot \bar{\mathbf{t}} d\Gamma - \int_{\Omega} \delta \mathbf{v} \cdot \bar{\mathbf{b}} d\Omega
\end{aligned} \tag{21e}$$

206 where the geometric relationships of Eq. (19) is used herein.

207 3. Mixed meshfree formulation for modified Hu-Washizu's weak form

208 3.1. Reproducing kernel approximation for displacement

209 This study approximates the displacement by adopting reproducing kernel
 210 approximation. As shown in Fig. 2, the mid-surface of the shell Ω is discretized
 211 by a set of meshfree nodes $\{\boldsymbol{\xi}_I\}_{I=1}^{n_p}$ in parametric configuration, where n_p is the
 212 total number of meshfree nodes. The approximated displacement namely \mathbf{v}^h
 213 can be expressed as:

$$\mathbf{v}(\boldsymbol{\xi}) = \sum_{I=1}^{n_p} \Psi_I(\boldsymbol{\xi}) \mathbf{d}_I \quad (22)$$

214 where Ψ_I and \mathbf{d}_I represent the shape function and nodal coefficient tensor re-
 215 lated by node $\boldsymbol{\xi}_I$. According to reproducing kernel approximation [20], the shape
 216 function takes the following form:

$$\Psi_I(\boldsymbol{\xi}) = \mathbf{p}^T(\boldsymbol{\xi}) \mathbf{c}(\boldsymbol{\xi}) \phi(\boldsymbol{\xi}_I - \boldsymbol{\xi}) \quad (23)$$

217 where \mathbf{p} is the basis function vector represented using the following quadratic
 218 function as:

$$\mathbf{p} = \{1, \xi^1, \xi^2, (\xi^1)^2, \xi^1 \xi^2, (\xi^2)^2\}^T \quad (24)$$

219 The kernel function denoted by ϕ controls the support and smoothness of
 220 meshfree shape functions. The quintic B-spline function with square support is
 221 used herein as the kernel function:

$$\phi(\boldsymbol{\xi}_I - \boldsymbol{\xi}) = \phi(\hat{s}_1) \phi(\hat{s}_2), \quad \hat{s}_\alpha = \frac{|\xi_I^\alpha - \xi^\alpha|}{s_{\alpha I}} \quad (25)$$

222 with

$$\phi(\hat{s}_\alpha) = \frac{1}{5!} \begin{cases} (3 - 3\hat{s}_\alpha)^5 - 6(2 - 3\hat{s}_\alpha)^5 + 15(1 - 3\hat{s}_\alpha)^5 & \hat{s}_\alpha \leq \frac{1}{3} \\ (3 - 3\hat{s}_\alpha)^5 - 6(2 - 3\hat{s}_\alpha)^5 & \frac{1}{3} < \hat{s}_\alpha \leq \frac{2}{3} \\ (3 - 3\hat{s}_\alpha)^5 & \frac{2}{3} < \hat{s}_\alpha \leq 1 \\ 0 & \hat{s}_\alpha > 1 \end{cases} \quad (26)$$

223 and $s_{\alpha I}$ means the support size of meshfree shape function Ψ_I .

224 The unknown vector \mathbf{c} in shape function are determined by the fulfillment
 225 of the so-called consistency condition:

$$\sum_{I=1}^{n_p} \Psi_I(\boldsymbol{\xi}) \mathbf{p}(\boldsymbol{\xi}_I) = \mathbf{p}(\boldsymbol{\xi}) \quad (27)$$

226 or equivalently

$$\sum_{I=1}^{n_p} \Psi_I(\boldsymbol{\xi}) \mathbf{p}(\boldsymbol{\xi}_I - \boldsymbol{\xi}) = \mathbf{p}(\mathbf{0}) \quad (28)$$

227 Substituting Eq. (22) into (28), yields:

$$\mathbf{A}(\boldsymbol{\xi}) \mathbf{c}(\boldsymbol{\xi}) = \mathbf{p}(\mathbf{0}) \quad \Rightarrow \quad \mathbf{c}(\boldsymbol{\xi}) = \mathbf{A}^{-1}(\boldsymbol{\xi}) \mathbf{p}(\mathbf{0}) \quad (29)$$

where \mathbf{A} is the moment matrix:

$$\mathbf{A}(\boldsymbol{\xi}) = \sum_{I=1}^{n_p} \phi(\boldsymbol{\xi}_I - \boldsymbol{\xi}) \mathbf{p}(\boldsymbol{\xi}_I - \boldsymbol{\xi}) \mathbf{p}^T(\boldsymbol{\xi}_I - \boldsymbol{\xi}) \quad (30)$$

Substituting Eq. (29) back into Eq. (22), the expression of meshfree shape function can be written as:

$$\Psi_I(\boldsymbol{\xi}) = \mathbf{p}^T(\boldsymbol{\xi}_I - \boldsymbol{\xi}) \mathbf{A}^{-1}(\boldsymbol{\xi}) \mathbf{p}(\mathbf{0}) \phi(\boldsymbol{\xi}_I - \boldsymbol{\xi}) \quad (31)$$

3.2. Reproducing kernel gradient smoothing approximation for effective stress and strain

In Galerkin meshfree formulation, the mid-plane of thin shell Ω is split by a set of integration cells Ω_C 's, $\cup_{C=1}^{n_c} \Omega_C \approx \Omega$, as shown in Fig. 2. With the inspiration of reproducing kernel smoothing framework, the Cartesian and covariant derivatives of displacement, $\mathbf{v}_{,\alpha}$ and $-\mathbf{v}_{,\alpha}|_{\beta}$, in strains $\varepsilon_{\alpha\beta}$, $\kappa_{\alpha\beta}$ are approximated by $(p-1)$ -th order polynomials in each integration cells. In integration cell Ω_C , the approximated derivatives and strains denoted by $\mathbf{v}_{,\alpha}^h$, $\varepsilon_{\alpha\beta}^h$ and $-\mathbf{v}_{,\alpha}^h|_{\beta}$, $\kappa_{\alpha\beta}^h$ can be expressed by:

$$\mathbf{v}_{,\alpha}^h(\boldsymbol{\xi}) = \mathbf{q}^T(\boldsymbol{\xi}) \mathbf{d}_{\alpha}^{\varepsilon}, \quad \varepsilon_{\alpha\beta}^h(\boldsymbol{\xi}) = \mathbf{q}^T(\boldsymbol{\xi}) \frac{1}{2} (\mathbf{a}_{\alpha} \cdot \mathbf{d}_{\beta}^{\varepsilon} + \mathbf{a}_{\beta} \cdot \mathbf{d}_{\alpha}^{\varepsilon}) \quad (32)$$

$$-\mathbf{v}_{,\alpha}^h|_{\beta}(\boldsymbol{\xi}) = \mathbf{q}^T(\boldsymbol{\xi}) \mathbf{d}_{\alpha\beta}^{\kappa}, \quad \kappa_{\alpha\beta}^h(\boldsymbol{\xi}) = \mathbf{q}^T(\boldsymbol{\xi}) \mathbf{a}_3 \cdot \mathbf{d}_{\alpha\beta}^{\kappa} \quad (33)$$

where \mathbf{q} is the linear polynomial vector and has the following form:

$$\mathbf{q} = \{1, \xi^1, \xi^2\}^T \quad (34)$$

and the $\mathbf{d}_{\alpha}^{\varepsilon}$, $\mathbf{d}_{\alpha\beta}^{\kappa}$ are the corresponding coefficient vector tensors. For the conciseness, the mixed usage of tensor and vector is introduced in this study. For instance, the component of coefficient tensor vector $\mathbf{d}_{\alpha I}^{\varepsilon}$, $\mathbf{d}_{\alpha}^{\varepsilon} = \{\mathbf{d}_{\alpha I}^{\varepsilon}\}$, is a three dimensional tensor, $\dim \mathbf{d}_{\alpha I}^{\varepsilon} = \dim \mathbf{v}$.

To satisfy the integration constraint of thin shell problem, the approximated stresses $N^{\alpha\beta h}$, $M^{\alpha\beta h}$ were assumed to have a comparable form to strains, and yields:

$$N^{\alpha\beta h}(\boldsymbol{\xi}) = \mathbf{q}^T(\boldsymbol{\xi}) \mathbf{a}^{\alpha} \cdot \mathbf{d}_N^{\beta}, \quad \mathbf{a}_{\alpha} N^{\alpha\beta h}(\boldsymbol{\xi}) = \mathbf{q}^T(\boldsymbol{\xi}) \mathbf{d}_N^{\beta} \quad (35)$$

$$M^{\alpha\beta h}(\boldsymbol{\xi}) = \mathbf{q}^T(\boldsymbol{\xi}) \mathbf{a}_3 \cdot \mathbf{d}_M^{\alpha\beta}, \quad \mathbf{a}_3 M^{\alpha\beta h}(\boldsymbol{\xi}) = \mathbf{q}^T(\boldsymbol{\xi}) \mathbf{d}_M^{\alpha\beta} \quad (36)$$

substituting the approximations of Eqs. (22), (32), (33), (35), (36) into Eqs. (21c), (21d) can express $\mathbf{d}_{\beta}^{\varepsilon}$ and $\mathbf{d}_{\alpha\beta}^{\kappa}$ by \mathbf{d} as:

$$\mathbf{d}_{\beta}^{\varepsilon} = \mathbf{G}^{-1} \left(\sum_{I=1}^{n_p} (\tilde{\mathbf{g}}_{\beta I} - \bar{\mathbf{g}}_{\beta I}) \mathbf{d}_I + \hat{\mathbf{g}}_{\beta} \right) \quad (37)$$

$$\mathbf{d}_{\alpha\beta}^{\kappa} = \mathbf{G}^{-1} \left(\sum_{I=1}^{n_p} (\tilde{\mathbf{g}}_{\alpha\beta I} - \bar{\mathbf{g}}_{\alpha\beta I}) \mathbf{d}_I + \hat{\mathbf{g}}_{\alpha\beta} \right) \quad (38)$$

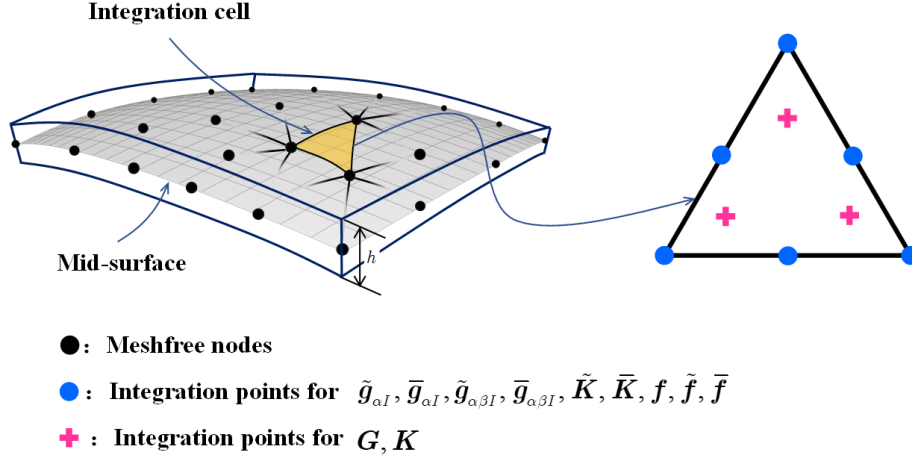


Figure 2: Integration scheme for Hu-Washizu weak form.

253 with

$$G = \int_{\Omega_C} \mathbf{q}^T \mathbf{q} d\Omega \quad (39)$$

254

$$\tilde{g}_{\beta I} = \int_{\Gamma_C} \Psi_I \mathbf{q} n_\beta d\Gamma - \int_{\Omega_C} \Psi_I \mathbf{q}_{|\beta} d\Omega \quad (40a)$$

$$\bar{g}_{\beta I} = \int_{\Gamma_C \cap \Gamma_v} \Psi_I \mathbf{q} n_\beta d\Gamma \quad (40b)$$

$$\hat{g}_\beta = \int_{\Gamma_C \cap \Gamma_v} \mathbf{q} n_\beta \bar{v} d\Gamma \quad (40c)$$

255

$$\begin{aligned} \tilde{g}_{\alpha\beta I} &= \int_{\Gamma_C} \Psi_{I,\gamma} n^\gamma \mathbf{q} n_\alpha n_\beta d\Gamma - \int_{\Gamma_C} \Psi_I (\mathbf{q}_{|\beta} n_\alpha + (\mathbf{q} s_\alpha n_\beta)_{,\gamma} s^\gamma) d\Gamma \\ &\quad + [[\Psi_I \mathbf{q} s_\alpha n_\beta]]_{\mathbf{x} \in C_C} - \int_{\Omega_C} \Psi \mathbf{q}_{,\alpha|\beta} d\Omega \end{aligned} \quad (41a)$$

$$\begin{aligned} \bar{g}_{\alpha\beta I} &= \int_{\Gamma_C \cap \Gamma_\theta} \Psi_{I,\gamma} n^\gamma \mathbf{q} n_\alpha n_\beta d\Gamma - \int_{\Gamma_C \cap \Gamma_v} \Psi_I (\mathbf{q}_{|\beta} n_\alpha + (\mathbf{q} s_\alpha n_\beta)_{,\gamma} s^\gamma) d\Gamma \\ &\quad + [[\Psi_I \mathbf{q} s_\alpha n_\beta]]_{\mathbf{x} \in C_C \cap C_v} \end{aligned} \quad (41b)$$

$$\begin{aligned} \hat{g}_{\alpha\beta} &= \int_{\Gamma_C \cap \Gamma_\theta} \mathbf{q} n_\alpha n_\beta \mathbf{a}_3 \bar{\theta}_n d\Gamma - \int_{\Gamma_C \cap \Gamma_v} (\mathbf{q}_{|\beta} n_\alpha + (\mathbf{q} s_\alpha n_\beta)_{,\gamma} s^\gamma) \bar{v} d\Gamma \\ &\quad + [[\mathbf{q} s_\alpha n_\beta \bar{v}]]_{\mathbf{x} \in C_C \cap C_v} \end{aligned} \quad (41c)$$

256 where evaluations of $\mathbf{q}_{|\beta}$, $\mathbf{q}_{,\alpha|\beta}$ are discussed in Appendix A. Further plugging
 257 Eqs. (37) and (38) back into Eqs. (32) and (33) respectively gives the final

258 expression of $\mathbf{v}_{,\alpha}^h$, $\varepsilon_{\alpha\beta}^h$ and $-\mathbf{v}_{,\alpha}^h|_{\beta}$, $\kappa_{\alpha\beta}^h$ as:

$$\mathbf{v}_{,\alpha}^h = \sum_{I=1}^{n_p} (\tilde{\Psi}_{I,\alpha} - \bar{\Psi}_{I,\alpha}) \mathbf{d}_I + \mathbf{q}^T \mathbf{G}^{-1} \hat{\mathbf{g}}_{\alpha} \quad (42a)$$

259

$$\begin{aligned} \varepsilon_{\alpha\beta}^h &= \sum_{I=1}^{n_p} \frac{1}{2} (\mathbf{a}_{\alpha} \tilde{\Psi}_{I,\beta} + \mathbf{a}_{\beta} \tilde{\Psi}_{I,\alpha}) \cdot \mathbf{d}_I - \sum_{I=1}^{n_p} \frac{1}{2} (\mathbf{a}_{\alpha} \bar{\Psi}_{I,\beta} + \mathbf{a}_{\beta} \bar{\Psi}_{I,\alpha}) \cdot \mathbf{d}_I \\ &\quad + \mathbf{q}^T \mathbf{G}^{-1} \frac{1}{2} (\mathbf{a}_{\alpha} \cdot \hat{\mathbf{g}}_{\beta} + \mathbf{a}_{\beta} \cdot \hat{\mathbf{g}}_{\alpha}) \\ &= \tilde{\varepsilon}_{\alpha\beta}^h - \bar{\varepsilon}_{\alpha\beta}^h + \hat{\varepsilon}_{\alpha\beta}^h \end{aligned} \quad (42b)$$

260

$$-\mathbf{v}_{,\alpha}^h|_{\beta} = \sum_{I=1}^{n_p} (\tilde{\Psi}_{I,\alpha\beta} - \bar{\Psi}_{I,\alpha\beta}) \mathbf{d}_I + \mathbf{q}^T \mathbf{G}^{-1} \hat{\mathbf{g}}_{\alpha\beta} \quad (43a)$$

261

$$\begin{aligned} \kappa_{\alpha\beta}^h &= \sum_{I=1}^{n_p} \tilde{\Psi}_{I,\alpha\beta} \mathbf{a}_3 \cdot \mathbf{d}_I - \sum_{I=1}^{n_p} \bar{\Psi}_{I,\alpha\beta} \mathbf{a}_3 \cdot \mathbf{d}_I + \mathbf{q}^T \mathbf{G}^{-1} \mathbf{a}_3 \cdot \hat{\mathbf{g}}_{\alpha\beta} \\ &= \tilde{\kappa}_{\alpha\beta}^h - \bar{\kappa}_{\alpha\beta}^h + \hat{\kappa}_{\alpha\beta}^h \end{aligned} \quad (43b)$$

262 with

$$\begin{cases} \tilde{\varepsilon}_{\alpha\beta}^h = \sum_{I=1}^{n_p} \frac{1}{2} (\mathbf{a}_{\alpha} \tilde{\Psi}_{I,\beta} + \mathbf{a}_{\beta} \tilde{\Psi}_{I,\alpha}) \cdot \mathbf{d}_I = \sum_{I=1}^{n_p} \tilde{\varepsilon}_{\alpha\beta I} \cdot \mathbf{d}_I \\ \bar{\varepsilon}_{\alpha\beta}^h = \sum_{I=1}^{n_p} \frac{1}{2} (\mathbf{a}_{\alpha} \bar{\Psi}_{I,\beta} + \mathbf{a}_{\beta} \bar{\Psi}_{I,\alpha}) \cdot \mathbf{d}_I = \sum_{I=1}^{n_p} \bar{\varepsilon}_{\alpha\beta I} \cdot \mathbf{d}_I \\ \hat{\varepsilon}_{\alpha\beta}^h = \mathbf{q}^T \mathbf{G}^{-1} \frac{1}{2} (\mathbf{a}_{\alpha} \cdot \hat{\mathbf{g}}_{\beta} + \mathbf{a}_{\beta} \cdot \hat{\mathbf{g}}_{\alpha}) \end{cases} \quad (44)$$

263

$$\begin{cases} \tilde{\Psi}_{I,\alpha}(\boldsymbol{\xi}) = \mathbf{q}^T(\boldsymbol{\xi}) \mathbf{G}^{-1} \tilde{\mathbf{g}}_{\alpha I} \\ \bar{\Psi}_{I,\alpha}(\boldsymbol{\xi}) = \mathbf{q}^T(\boldsymbol{\xi}) \mathbf{G}^{-1} \bar{\mathbf{g}}_{\alpha I} \\ \tilde{\varepsilon}_{\alpha\beta I} = \frac{1}{2} (\mathbf{a}_{\alpha} \tilde{\Psi}_{I,\beta} + \mathbf{a}_{\beta} \tilde{\Psi}_{I,\alpha}) \\ \bar{\varepsilon}_{\alpha\beta I} = \frac{1}{2} (\mathbf{a}_{\alpha} \bar{\Psi}_{I,\beta} + \mathbf{a}_{\beta} \bar{\Psi}_{I,\alpha}) \end{cases} \quad (45)$$

264

$$\begin{cases} \tilde{\kappa}_{\alpha\beta}^h = \sum_{I=1}^{n_p} \tilde{\Psi}_{I,\alpha\beta} \mathbf{a}_3 \cdot \mathbf{d}_I = \sum_{I=1}^{n_p} \tilde{\kappa}_{\alpha\beta I} \cdot \mathbf{d}_I \\ \bar{\kappa}_{\alpha\beta}^h = \sum_{I=1}^{n_p} \bar{\Psi}_{I,\alpha\beta} \mathbf{a}_3 \cdot \mathbf{d}_I = \sum_{I=1}^{n_p} \bar{\kappa}_{\alpha\beta I} \cdot \mathbf{d}_I \\ \hat{\kappa}_{\alpha\beta}^h = \mathbf{q}^T \mathbf{G}^{-1} \mathbf{a}_3 \cdot \hat{\mathbf{g}}_{\alpha\beta} \end{cases} \quad (46)$$

265

$$\begin{cases} \tilde{\Psi}_{I,\alpha\beta}(\boldsymbol{\xi}) = \mathbf{q}^T(\boldsymbol{\xi}) \mathbf{G}^{-1} \tilde{\mathbf{g}}_{\alpha\beta I} \\ \bar{\Psi}_{I,\alpha\beta}(\boldsymbol{\xi}) = \mathbf{q}^T(\boldsymbol{\xi}) \mathbf{G}^{-1} \bar{\mathbf{g}}_{\alpha\beta I} \\ \tilde{\kappa}_{\alpha\beta I} = \tilde{\Psi}_{I,\alpha\beta} \mathbf{a}_3 \\ \bar{\kappa}_{\alpha\beta I} = \bar{\Psi}_{I,\alpha\beta} \mathbf{a}_3 \end{cases} \quad (47)$$

266 It has to be noted that, referring to reproducing kernel gradient smoothing
 267 framework [35], $\tilde{\Psi}_{I,\alpha}$, $\tilde{\Psi}_{I,\alpha\beta}$ are actually the first and second order smoothed
 268 gradients in curvilinear coordinates. If the right hand side integration constraints
 269 for first and second order gradients are $\tilde{\mathbf{g}}_{\alpha I}$ and $\tilde{\mathbf{g}}_{\alpha\beta I}$, respectively, then this for-
 270 mulation can satisfy the variational consistency for the second order polynomi-
 271 als. It should be mentioned that in curved model, the variational consistency for
 272 non-polynomial functions, such as trigonometric functions, should be required
 273 for the polynomial solution. Even with high order polynomial variational consis-
 274 tency, the proposed formulation cannot exactly reproduce the solution spanned
 275 by the basis functions. However, the accuracy of reproducing kernel smoothed
 276 gradients is still superior than the traditional meshfree formulation. The nu-
 277 merical examples in the following section will better demonstrate the precision
 278 of the reproducing kernel smoothed gradients.

279 **4. Naturally variational enforcement for essential boundary condi-**
 280 **tions**

281 *4.1. Discrete equilibrium equations*

282 With the approximated effective stresses and strains, the last equation of
 283 weak form Eq. (21e) becomes:

$$-\sum_{C=1}^{n_e} \sum_{I=1}^{n_p} \delta \mathbf{d}_I \cdot \left((\tilde{\mathbf{g}}_{\alpha I}^T - \bar{\mathbf{g}}_{\alpha I}^T) \mathbf{d}_N^\alpha + (\tilde{\mathbf{g}}_{\alpha \beta I}^T - \bar{\mathbf{g}}_{\alpha \beta I}^T) \mathbf{d}_M^{\alpha \beta} \right) = -\sum_{I=1}^{n_p} \delta \mathbf{d}_I \cdot \mathbf{f}_I \quad (48)$$

284 where \mathbf{f}_I 's denote the components of the traditional force vector:

$$\mathbf{f}_I = \int_{\Gamma_t} \Psi_I \bar{\mathbf{t}} d\Gamma - \int_{\Gamma_M} \Psi_{I,\gamma} n^\gamma \bar{M}_{nn} d\Gamma + [[\Psi_I \mathbf{a}_3 \bar{P}]]_{\mathbf{x} \in C_P} + \int_{\Omega} \Psi_I \bar{\mathbf{b}} d\Omega \quad (49)$$

285 The left side of Eq. (48) can be simplified using the following steps. For clarity,
 286 the derivation of first term in Eq. (48) taken as an example is given by:

$$\begin{aligned} \sum_{I=1}^{n_p} \delta \mathbf{d}_I \cdot \tilde{\mathbf{g}}_{\alpha I}^T \mathbf{d}_N^\alpha &= \sum_{I=1}^{n_p} \delta \mathbf{d}_I \cdot (\mathbf{G}^{-1} \tilde{\mathbf{g}}_{\alpha I})^T \mathbf{G} \mathbf{d}_N^\alpha \\ &= \int_{\Omega_C} \sum_{I=1}^{n_p} \delta \mathbf{d}_I \cdot (\mathbf{q}^T \mathbf{G}^{-1} \tilde{\mathbf{g}}_{\alpha I}) \mathbf{q}^T \mathbf{d}_N^\alpha d\Omega \\ &= \int_{\Omega_C} \sum_{I=1}^{n_p} \delta \mathbf{d}_I \cdot \mathbf{a}_\beta (\mathbf{q}^T \mathbf{G}^{-1} \tilde{\mathbf{g}}_{\alpha I}) N^{\alpha \beta h} d\Omega \\ &= \int_{\Omega_C} \delta \tilde{\varepsilon}_{\alpha \beta}^h N^{\alpha \beta h} d\Omega \end{aligned} \quad (50)$$

287 following the above procedure and including the weak form of Eqs. (21a), (21b),
 288 the left side of Eq. (48) in Ω_C becomes:

$$\begin{aligned}
 & \sum_{I=1}^{n_p} \delta \mathbf{d}_I \cdot \left((\tilde{\mathbf{g}}_{\alpha I}^T - \bar{\mathbf{g}}_{\alpha I}^T) \mathbf{d}_N^\alpha + (\tilde{\mathbf{g}}_{\alpha \beta I}^T - \bar{\mathbf{g}}_{\alpha \beta I}^T) \mathbf{d}_M^{\alpha \beta} \right) \\
 &= \int_{\Omega_C} ((\delta \tilde{\varepsilon}_{\alpha \beta}^h - \delta \bar{\varepsilon}_{\alpha \beta}^h) N^{\alpha \beta h} + (\delta \tilde{\kappa}_{\alpha \beta}^h - \delta \bar{\kappa}_{\alpha \beta}^h) M^{\alpha \beta h}) d\Omega \\
 &= \int_{\Omega_C} (\delta \tilde{\varepsilon}_{\alpha \beta}^h - \delta \bar{\varepsilon}_{\alpha \beta}^h) h C^{\alpha \beta \gamma \eta} \varepsilon_{\gamma \eta}^h + (\delta \tilde{\kappa}_{\alpha \beta}^h - \delta \bar{\kappa}_{\alpha \beta}^h) \frac{h^3}{12} C^{\alpha \beta \gamma \eta} \kappa_{\gamma \eta}^h \\
 &= \int_{\Omega_C} \delta \tilde{\varepsilon}_{\alpha \beta}^h h C^{\alpha \beta \gamma \eta} \varepsilon_{\gamma \eta}^h d\Omega + \int_{\Omega_C} \delta \tilde{\kappa}_{\alpha \beta}^h \frac{h^3}{12} C^{\alpha \beta \gamma \eta} \kappa_{\gamma \eta}^h d\Omega \\
 &\quad - \int_{\Omega_C} \delta \bar{\varepsilon}_{\alpha \beta}^h h C^{\alpha \beta \gamma \eta} \varepsilon_{\gamma \eta}^h d\Omega - \int_{\Omega_C} \delta \bar{\kappa}_{\alpha \beta}^h h C^{\alpha \beta \gamma \eta} \varepsilon_{\gamma \eta}^h d\Omega \\
 &\quad - \int_{\Omega_C} \delta \tilde{\kappa}_{\alpha \beta}^h \frac{h^3}{12} C^{\alpha \beta \gamma \eta} \kappa_{\gamma \eta}^h d\Omega - \int_{\Omega_C} \delta \bar{\kappa}_{\alpha \beta}^h \frac{h^3}{12} C^{\alpha \beta \gamma \eta} \kappa_{\gamma \eta}^h d\Omega \\
 &\quad + \int_{\Omega_C} \delta \bar{\varepsilon}_{\alpha \beta}^h h C^{\alpha \beta \gamma \eta} \varepsilon_{\gamma \eta}^h d\Omega + \int_{\Omega_C} \delta \bar{\kappa}_{\alpha \beta}^h \frac{h^3}{12} C^{\alpha \beta \gamma \eta} \kappa_{\gamma \eta}^h d\Omega \\
 &\quad + \int_{\Omega_C} (\delta \tilde{\varepsilon}_{\alpha \beta}^h - \delta \bar{\varepsilon}_{\alpha \beta}^h) h C^{\alpha \beta \gamma \eta} \varepsilon_{\gamma \eta}^h d\Omega + \int_{\Omega_C} (\delta \tilde{\kappa}_{\alpha \beta}^h - \delta \bar{\kappa}_{\alpha \beta}^h) \frac{h^3}{12} C^{\alpha \beta \gamma \eta} \kappa_{\gamma \eta}^h d\Omega
 \end{aligned} \tag{51}$$

289 The complete discrete equilibrium equations can be obtained by further substituting
 290 Eqs. (44) and (46) into above equation, respectively:

$$(\mathbf{K} + \tilde{\mathbf{K}} + \bar{\mathbf{K}}) \mathbf{d} = \mathbf{f} + \tilde{\mathbf{f}} + \bar{\mathbf{f}} \tag{52}$$

291 where the components of stiffness matrices and force vectors in discrete equilibrium
 292 equations can be evaluated as follows:

$$\mathbf{K}_{IJ} = \int_{\Omega} \tilde{\varepsilon}_{\alpha \beta I} h C^{\alpha \beta \gamma \eta} \tilde{\varepsilon}_{\gamma \eta J} d\Omega + \int_{\Omega} \tilde{\kappa}_{\alpha \beta I} \frac{h^3}{12} C^{\alpha \beta \gamma \eta} \tilde{\kappa}_{\gamma \eta J} d\Omega \tag{53}$$

293

$$\begin{aligned}
 \tilde{\mathbf{K}}_{IJ} &= - \int_{\Gamma_v} (\Psi_I \tilde{\mathbf{T}}_{NJ} + \tilde{\mathbf{T}}_{NI} \Psi_J) d\Gamma \\
 &\quad + \int_{\Gamma_\theta} (\Psi_{I,\gamma} n^\gamma \mathbf{a}_3 \tilde{\mathbf{M}}_{nnJ} + \mathbf{a}_3 \tilde{\mathbf{M}}_{nnI} \Psi_{J,\gamma} n^\gamma) d\Gamma \\
 &\quad + ([[\Psi_I \mathbf{a}_3 \tilde{\mathbf{P}}_J]] + [[\tilde{\mathbf{P}}_I \mathbf{a}_3 \Psi_J]])_{\mathbf{x} \in C_v}
 \end{aligned} \tag{54a}$$

$$\tilde{\mathbf{f}}_I = - \int_{\Gamma_v} \tilde{\mathbf{T}}_{NI} \cdot \bar{\mathbf{v}} d\Gamma + \int_{\Gamma_\theta} \tilde{\mathbf{M}}_{nnI} \bar{\theta}_n d\Gamma + [[\tilde{\mathbf{P}}_I \mathbf{a}_3 \cdot \bar{\mathbf{v}}]]_{\mathbf{x} \in C_v} \tag{54b}$$

294

$$\bar{\mathbf{K}}_{IJ} = - \int_{\Gamma_v} \bar{\mathbf{T}}_{MI} \Psi_J d\Gamma + \int_{\Gamma_\theta} \mathbf{a}_3 \bar{\mathbf{M}}_{nnI} \Psi_{J,\gamma} n^\gamma d\Gamma + [[\bar{\mathbf{P}}_I \mathbf{a}_3 \Psi_J]]_{\mathbf{x} \in C_v} \tag{55a}$$

$$\bar{\mathbf{f}}_I = - \int_{\Gamma_v} \bar{\mathbf{T}}_{MI} \cdot \bar{\mathbf{v}} d\Gamma + \int_{\Gamma_\theta} \bar{\mathbf{M}}_{nnI} \bar{\theta}_n d\Gamma + [[\bar{\mathbf{P}}_I \mathbf{a}_3 \cdot \bar{\mathbf{v}}]]_{\mathbf{x} \in C_v} \tag{55b}$$

295 The detailed derivations of Eqs (53)-(55) are listed in the Appendix B. As
 296 shown in these equations, Eq. (53) is the conventional stiffness matrix evalu-
 297 ated by smoothed gradients $\tilde{\Psi}_{I,\alpha}$, $\tilde{\Psi}_{I,\alpha|\beta}$, and the Eqs. (54) and (55) contribute
 298 for the enforcement of essential boundary. It should be noticed that, in accor-
 299 dance with reproducing kernel smoothed gradient framework, the integration
 300 scheme of Eqs. (53-55) should be aligned with those used in the construction of
 301 smoothed gradients. The integration scheme used for the proposed method is
 302 shown in Fig. 2, in which the total number of the blue circular integration points
 303 has been optimized from a global point of view, aiming to reduce the compu-
 304 tation of traditional meshfree shape functions and its first order derivatives. In
 305 contrast, for assembly stiffness matrix \mathbf{K} , the low order Gauss integration rule
 306 is suitable to ensure the accuracy due to the inherently variational consistency
 307 in the smoothed gradients. The detailed positions and weight of the integration
 308 points and the efficiency demonstration of this optimized integration scheme
 309 can be found in [35, 41]. Examining Eqs. (54) and (55), closely reveal that the
 310 structure of the suggested approach to enforce essential boundary conditions is
 311 identical to that of the conventional Nitsche's method, with both having the
 312 consistent and stabilized terms. Thus, a review of Nitsche's method and a com-
 313 parison with the proposed approach will be provided in the next subsection.

314 4.2. Comparison with Nitsche's method

315 The Nitsche's method for enforcing essential boundaries can be regarded as a
 316 combination of Lagrangian multiplier method and penalty method, in which the
 317 Lagrangian multiplier is represented by the approximated displacement. The
 318 corresponding total potential energy functional Π_P is given by:

$$\begin{aligned}
 \Pi_P(\mathbf{v}) = & \int_{\Omega} \frac{1}{2} \varepsilon_{\alpha\beta} N^{\alpha\beta} d\Omega + \int_{\Omega} \frac{1}{2} \kappa_{\alpha\beta} M^{\alpha\beta} d\Omega \\
 & - \int_{\Gamma_t} \mathbf{v} \cdot \bar{\mathbf{t}} d\Gamma + \int_{\Gamma_M} \mathbf{v}_{,\gamma} n^{\gamma} \mathbf{a}_3 M_{nn} d\Gamma + (\mathbf{v} \cdot \mathbf{a}_3 P)_{\mathbf{x} \in C_P} - \int_{\Omega} \mathbf{v} \cdot \bar{\mathbf{b}} d\Omega \\
 & - \underbrace{\int_{\Gamma_v} \mathbf{t} \cdot (\mathbf{v} - \bar{\mathbf{v}}) d\Gamma + \int_{\Gamma_{\theta}} M_{nn} (\theta_n - \bar{\theta}_n) d\Gamma + (P \mathbf{a}_3 \cdot (\mathbf{v} - \bar{\mathbf{v}}))_{\mathbf{x} \in C_v}}_{\text{consistent term}} \quad (56) \\
 & + \underbrace{\sum_{i=1}^3 \frac{\alpha_{vi}}{2} \int_{\Gamma_v} (\mathbf{v} \cdot \mathbf{a}_i)^2 d\Gamma + \frac{\alpha_{\theta}}{2} \int_{\Gamma_{\theta}} \theta_n^2 d\Gamma + \frac{\alpha_C}{2} (\mathbf{v} \cdot \mathbf{a}_3)_{\mathbf{x} \in C_v}^2}_{\text{stabilized term}}
 \end{aligned}$$

319 where the consistent term generated from the Lagrangian multiplier method
 320 contributes to enforce the essential boundary, and meet the variational con-
 321 sistency condition. However, the consistent term can not always ensure the
 322 coercivity of stiffness, so the penalty method is introduced to serve as a sta-
 323 bilized term, in which α_{vi} is the experimental artificial parameter to enforce
 324 the displacement towards the \mathbf{a}_i direction, α_{θ} and α_C are parameters to en-
 325 force rotation and corner deflection, respectively. With a standard variational

argument, the corresponding weak form can be stated as:

$$\begin{aligned}
\delta \Pi_P(\mathbf{v}) = & \int_{\Omega} \delta \varepsilon_{\alpha\beta} N^{\alpha\beta} d\Omega + \int_{\Omega} \delta \kappa_{\alpha\beta} M^{\alpha\beta} d\Omega \\
& - \int_{\Gamma_t} \delta \mathbf{v} \cdot \bar{\mathbf{t}} d\Gamma + \int_{\Gamma_M} \delta \mathbf{v}_{,\gamma} n^{\gamma} \mathbf{a}_3 M_{nn} d\Gamma + (\delta \mathbf{v} \cdot \mathbf{a}_3 P)_{\mathbf{x} \in C_P} - \int_{\Omega} \delta \mathbf{v} \cdot \bar{\mathbf{b}} d\Omega \\
& - \int_{\Gamma_v} \delta \mathbf{v} \cdot \mathbf{t} d\Gamma + \int_{\Gamma_{\theta}} \delta \theta_{\mathbf{n}} M_{nn} d\Gamma + (\mathbf{v} \cdot \mathbf{a}_3 P)_{\mathbf{x} \in C_v} \\
& - \int_{\Gamma_v} \delta \mathbf{t} \cdot (\mathbf{v} - \bar{\mathbf{v}}) d\Gamma + \int_{\Gamma_{\theta}} \delta M_{nn} (\theta_{\mathbf{n}} - \bar{\theta}_{\mathbf{n}}) d\Gamma + (\delta P \mathbf{a}_3 \cdot (\mathbf{v} - \bar{\mathbf{v}}))_{\mathbf{x} \in C_v} \\
& + \sum_{i=1}^3 \alpha_{vi} \int_{\Gamma_v} (\delta \mathbf{v} \cdot \mathbf{a}_i) (\mathbf{a}_i \cdot \mathbf{v}) d\Gamma + \alpha_{\theta} \int_{\Gamma_{\theta}} \delta \theta_{\mathbf{n}} \theta_{\mathbf{n}} d\Gamma + \alpha_C (\delta \mathbf{v} \cdot \mathbf{a}_3 \mathbf{a}_3 \cdot \mathbf{v})_{\mathbf{x} \in C_v} \\
& = 0
\end{aligned} \tag{57}$$

Upon further invoking the conventional reproducing kernel approximation of Eq. (22), the subsequent discrete equilibrium equations can be obtained:

$$(\mathbf{K} + \mathbf{K}^c + \mathbf{K}^s) \mathbf{d} = \mathbf{f} + \mathbf{f}^c + \mathbf{f}^s \tag{58}$$

where the stiffness \mathbf{K} is identical with Eq. (53). \mathbf{K}^c and \mathbf{K}^s are the stiffness matrices for consistent and stabilized terms, respectively, and their components have the following form:

$$\begin{aligned}
\mathbf{K}_{IJ}^c = & - \int_{\Gamma_v} (\Psi_I \mathbf{T}_{NJ} + \mathbf{T}_{NI} \Psi_J) d\Gamma \\
& + \int_{\Gamma_{\theta}} (\Psi_{I,\gamma} n^{\gamma} \mathbf{a}_3 M_{nnJ} + \mathbf{a}_3 M_{nnI} \Psi_{J,\gamma} n^{\gamma}) d\Gamma \\
& + ([\Psi_I \mathbf{a}_3 P_J] + [P_I \mathbf{a}_3 \Psi_J])_{\mathbf{x} \in C_v}
\end{aligned} \tag{59a}$$

$$\mathbf{f}_I^c = - \int_{\Gamma_v} \mathbf{T}_I \cdot \bar{\mathbf{v}} d\Gamma + \int_{\Gamma_{\theta}} M_{nnI} \bar{\theta}_{\mathbf{n}} d\Gamma + [P_I \mathbf{a}_3 \cdot \bar{\mathbf{v}}]_{\mathbf{x} \in C_v} \tag{59b}$$

$$\mathbf{K}_{IJ}^s = \alpha_v \int_{\Gamma_v} \Psi_I \Psi_J d\Gamma + \alpha_{\theta} \int_{\Gamma_{\theta}} \Psi_{I,\eta} n^{\eta} \mathbf{a}_3 \mathbf{a}_3 n^{\gamma} \Psi_{J,\gamma} d\Gamma + \alpha_C [\Psi_I \mathbf{a}_3 \mathbf{a}_3 \Psi_J]_{\mathbf{x} \in C_v} \tag{60a}$$

$$\mathbf{f}_I^s = \alpha_v \int_{\Gamma_v} \Psi_I \bar{\mathbf{v}} d\Gamma + \alpha_{\theta} \int_{\Gamma_{\theta}} \Psi_{I,\eta} n^{\eta} \mathbf{a}_3 \bar{\theta}_{\mathbf{n}} d\Gamma + \alpha_C [\Psi_I \mathbf{a}_3 \mathbf{a}_3 \cdot \bar{\mathbf{v}}]_{\mathbf{x} \in C_v} \tag{60b}$$

with

$$\boldsymbol{\alpha}_v = \begin{bmatrix} \alpha_{v1} & 0 & 0 \\ 0 & \alpha_{v2} & 0 \\ 0 & 0 & \alpha_{v3} \end{bmatrix} \tag{61}$$

On comparing with the consistent terms of Eqs. (54) and (59), the expressions were almost identical, the major difference is that the higher order

336 derivatives of shape functions have been replaced by the smoothed gradients.
 337 Owing to the reproducing kernel framework, the construction of the smoothed
 338 gradients only concerned about the computation of traditional meshfree shape
 339 functions and their first order derivatives, which avoid the costly computation
 340 of higher order derivatives. Moreover, the stabilized terms in Eq. (60) em-
 341 ploys the penalty method with big enough artificial parameters to ensure the
 342 coercivity of stiffness. Besides, the optimal values of these artificial parame-
 343 ters are proportional to the grid size of discrete model that can be represented
 344 by the support size in meshfree approximation, where $\alpha_{v\alpha} \propto s^{-1}$, $\alpha_{v3} \propto s^{-3}$,
 345 $\alpha_\theta \propto s^{-1}$, $\alpha_C \propto s^{-2}$ [39], and $s = \min\{s_{\alpha I}\}$. In contrast, the stabilized term of
 346 Eq. (55) naturally exists in its weak form, and can stabilize the result without
 347 considering any artificial parameters.

348 5. Numerical examples

349 In this section, the suggested method is validated through several exam-
 350 ples using the Nitsche's method, the consistent reproducing kernel gradient
 351 smoothing integration scheme (RKGSI), and the non-consistent Gauss inte-
 352 gration scheme (GI) with penalty method, as well as the proposed Hu-Washizu
 353 formulation (HW) to enforce the necessary boundary conditions. A normalized
 354 support size of 2.5 is used for all the considered methods to ensure the require-
 355 ment of quadratic base meshfree approximation. To eliminate the influence of
 356 integration error, the Gauss integration scheme uses 6 Gauss points for domain
 357 integration and 3 points for boundary integration, so as to maintain the same
 358 integration accuracy between domain and boundaries. Moreover, the number
 359 of integration points are identical between the Gauss and RKGSI schemes. The
 360 error estimates of displacement (L_2 -Error) and energy (H_e -Error) is used here:

$$\begin{aligned}
 L_2\text{-Error} &= \frac{\sqrt{\int_{\Omega} (\mathbf{v} - \mathbf{v}^h) \cdot (\mathbf{v} - \mathbf{v}^h) d\Omega}}{\sqrt{\mathbf{v} \cdot \mathbf{v}}} \\
 H_e\text{-Error} &= \frac{\sqrt{\int_{\Omega} \left((\varepsilon_{\alpha\beta} - \varepsilon_{\alpha\beta}^h)(N^{\alpha\beta} - N^{\alpha\beta h}) + \int_{\Omega} (\kappa_{\alpha\beta} - \kappa_{\alpha\beta}^h)(M^{\alpha\beta} - M^{\alpha\beta h}) \right) d\Omega}}{\sqrt{\int_{\Omega} (\varepsilon_{\alpha\beta} N^{\alpha\beta} + \kappa_{\alpha\beta} M^{\alpha\beta}) d\Omega}}
 \end{aligned} \tag{62}$$

361 5.1. Patch tests

362 The linear and quadratic patch tests for flat and curved thin shells are firstly
 363 studied to verify the variational consistency of the proposed method. As shown
 364 in Fig. 3, the flat and curved models are depicted by an identical parametric
 365 domain $\Omega = (0, 1) \otimes (0, 1)$, where the cylindrical coordinate system with radius
 366 $R = 1$, thickness ~~$h = 0.1$~~ $h = 0.05$ is employed to describe the curved model,
 367 and the whole domain Ω is discretized by the 165 meshfree nodes. The Young's
 368 modulus and Poisson's ratio of thin shell are set to $E = 1$, $\nu = 0$. The artificial
 369 parameters of $\alpha_v = 10^5 \times E$, $\alpha_\theta = 10^3 \times E$, $\alpha_C = 10^5 \times E$ and $\alpha_v = 10^9 \times$
 370 E , $\alpha_\theta = 10^9 \times E$, $\alpha_C = 10^9 \times E$ were adopted in Nitsche's- and penalty- method,
 371 respectively. All the boundaries are enforced as essential boundary conditions
 372 with the following manufactured exact solution:

$$\mathbf{v} = \begin{Bmatrix} (\xi^1 + 2\xi^2)^n \\ (3\xi^1 + 4\xi^2)^n \\ (5\xi^1 + 6\xi^2)^n \end{Bmatrix}, \quad n = \begin{cases} 1 & \text{Linear patch test} \\ 2 & \text{Quadratic patch test} \end{cases} \tag{63}$$

373 Table 1 lists the L_2 - and H_e -Error results of patch test with flat model, where
 374 the RKGSI scheme with variational consistent essential boundary enforcement,
 375 i.e. RKGSI-Nitsche and RKGSI-HW, can pass the linear and quadratic patch
 376 test. In contrast, the RKGSI-Penalty cannot pass the patch test since the
 377 Penalty method is unable to ensure the variational consistency. Due to the
 378 loss of variational consistency condition, even with the Nitsche's method, Gauss

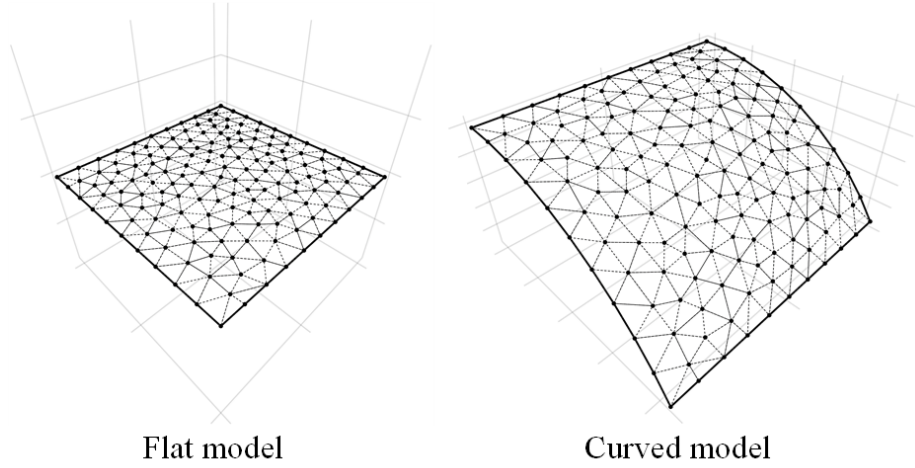


Figure 3: Meshfree discretization for patch test

379 meshfree formulations show noticeable errors. Table 2 shows the results for
 380 curved model, which indicated that all the considered methods cannot pass
 381 the patch test. This is mainly because the proposed smoothed gradient of
 382 Eqs. (35) and (36) could not exactly reproduce the non-polynomial membrane
 383 and bending stresses. On the other hand, the RKGSI-HW and RKGSI-Nitsche
 384 methods provide better accuracy compared to the other approaches due to the
 385 fulfillment of first second-order variational consistency. Even only with local
 386 variational consistency, the RKGSI-Penalty obtained a better result than the
 387 traditional Gauss scheme. Meanwhile, the bending moment contours of M^{12}
 388 are listed in Fig. 4, which further verify that the proposed method provided a
 389 satisfactory result compared to the exact solution. Contrarily, both the RKGSI-
 390 Penalty and the conventional Gauss meshree formulations observed errors.

Table 1: Results of patch test for flat model.

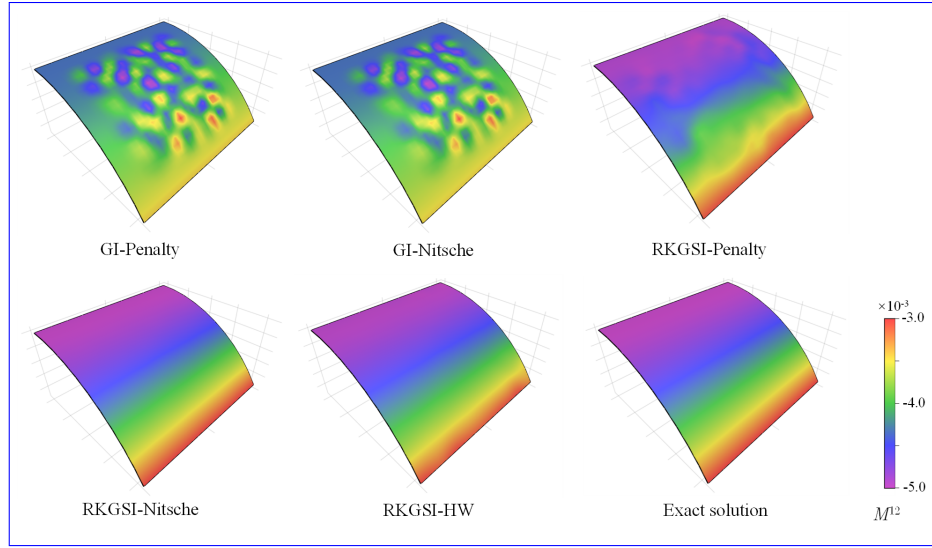
	Linear patch test		Quadratic patch test	
	L_2 -Error	H_e -Error	L_2 -Error	H_e -Error
GI-Penalty	4.45 <u>1.41</u> E-04	1.35E-02 <u>4.62E-03</u>	2.01 <u>1.97</u> E-03	1.63E-02 <u>7.17E-03</u>
GI-Nitsche	4.51 <u>1.73</u> E-04	1.42E-02 <u>5.61E-03</u>	1.22 <u>1.85</u> E-03	1.68E-02 <u>7.76E-03</u>
RKGSI-Penalty	3.64 <u>5.04</u> E-09	6.77E-08 <u>1.02E-07</u>	4.54 <u>3.01</u> E-09	6.57 <u>3.41</u> E-08
RKGSI-Nitsche	3.31 <u>9.75</u> E-12	1.34 <u>8.98</u> E-11	5.98 <u>1.29</u> E-12	1.21E-11 <u>1.06E-12</u>
RKGSI-HR	6.67 <u>6.15</u> E-13	1.50E-11 <u>1.07</u> <u>6.91</u> E-12	1.26E-11 <u>7.51E-13</u>	8.36E-12

391 5.2. Scordelis-Lo roof

392 This example considers the classical Scordelis-Lo roof problem, as depicted
 393 in Fig. 5. The cylindrical roof has dimensions $R = 25$, $L = 50$, $h = 0.25$,

Table 2: Results of patch test for cylindrical model.

	Linear patch test		Quadratic patch test	
	L_2 -Error	H_e -Error	L_2 -Error	H_e -Error
GI-Penalty	3.79 1.75E-04	1.30E-02 4.50E-03	1.74 1.08E-03	1.37E-02 5.83E-03
GI-Nitsche	4.04 1.77E-04	1.42E-02 5.36E-03	1.15 1.07E-03	1.49E-02 6.33E-03
RKGSi-Penalty	1.47 8.59E-05	9.11E-04	5.39E-03 2.264.28E-04	2.09 2.08E-03
RKGSi-Nitsche	2.41E-06 1.27E-05	7.37 5.32E-05	2.47E-06 2.891.88E-05	5.6E-04
RKGSi-HR	4.28E-06 1.43E-05	1.30 1.60E-04	9.69E-06 2.93E-05	2.41 2.85E-04

Figure 4: Contour plots of M^{12} for curved shell patch test.

394 Young's modulus $E = 4.32 \times 10^8$ and Poisson's ratio $\nu = 0.0$. The entire roof
395 is subjected to ~~an a~~ uniform body force of $b_z = -90$, with the straight edges
396 ~~remaining-remaining~~ free and the ~~the~~ curved edges are enforced by $v_x = v_z = 0$.

397 Due to the symmetry, only a quadrant of the model is considered for meshfree
398 analysis, which is discretized by the 11×16 , 13×20 , 17×24 and 19×28 meshfree
399 nodes, as listed in Fig. 6. The comparison of the displacement in z -direction
400 at node A , v_{A3} , is used as the investigated quantity, with the reference value
401 ~~0.3006~~-0.3006 given by [9]. Firstly, Fig. 7 presents a sensitivity study for the
402 artificial parameters of α_{vi} 's and α_θ 's in the RKGSi meshfree formulations with
403 the Nitsche's- and penalty- method, where all ~~of~~ the parameters are scaled by
404 the support size as, $\alpha_{v\alpha} = s^{-1}\bar{\alpha}_v$, $\alpha_{v3} = s^{-3}\bar{\alpha}_v$ and $\alpha_\theta = s^{-1}\bar{\alpha}_\theta$. For a better
405 comparison, the result of the proposed RKGSi-HW is also listed in this figure.
406 The results of Fig. 7 revealed, that Nitsche's method observed less artificial
407 sensitivity. However, both the methods cannot trivially determine the optimal
408 values of the artificial parameters. The optimal artificial parameters from Fig.

7 are adopted for the convergence study in Fig. 8. The convergence result showed that the RKGSi method get satisfactory results while the traditional Gauss methods demonstrated noticeable errors.

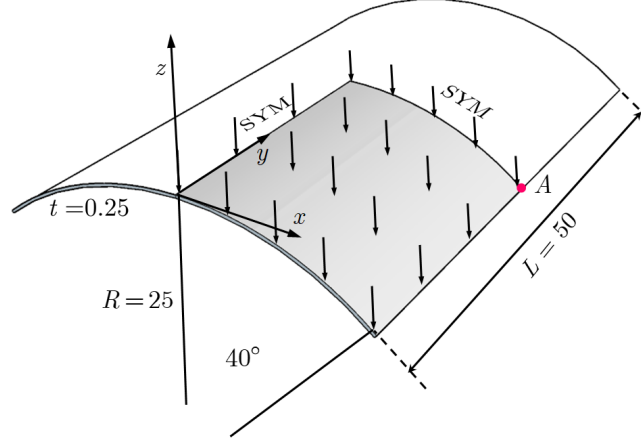


Figure 5: Description of Scordelis-Lo roof problem.

5.3. Pinched Hemispherical shell

Consider the hemispherical shell shown in Fig. 9, which is loaded at four points $P = \pm 2$ at 90° interval at its bottom. The hemispherical shell has a radius $R = 10$, thickness $h = 0.04$, Young's modulus $E = 6.825 \times 10^7$ and Poisson's ratio $\nu = 0.3$.

Due to symmetry, only quadrant model, where the 16×16 , 24×24 , 32×32 and 40×40 meshfree nodes have been discretized as shown in Fig. (10), were considered. The quantity under investigation for convergence is the displacement at x -direction on point A, $v_{A1} = 0.094$ [42]. Fig. 11 displays the corresponding convergence results, indicating the RKGSi scheme performed significantly better compared to the GI meshfree formulation. Meanwhile, the efficiency comparison for this problem is also shown in Fig. 12, in which the CPU time for assembly and calculation of shape functions are considered. Fig. 12(a) indicates that the RKGSi scheme observed high efficiency in assembly. This is due to the variational inconsistent Gauss meshfree formulation which require more Gaussian points to get satisfactory results. Fig. 12(b) lists the CPU time spent on enforcing essential boundary conditions for the penalty method, Nitsche's method and proposed HW method. The results highlighted that the proposed HW method consumed comparable CPU time in assembly compared to Nitsche's method. However, less time was spent to calculate the shape functions. Since both the HW method and penalty method were developed considering the shape functions first order derivatives. For this reason, both the methods shared an almost identical time in computing the shape functions.

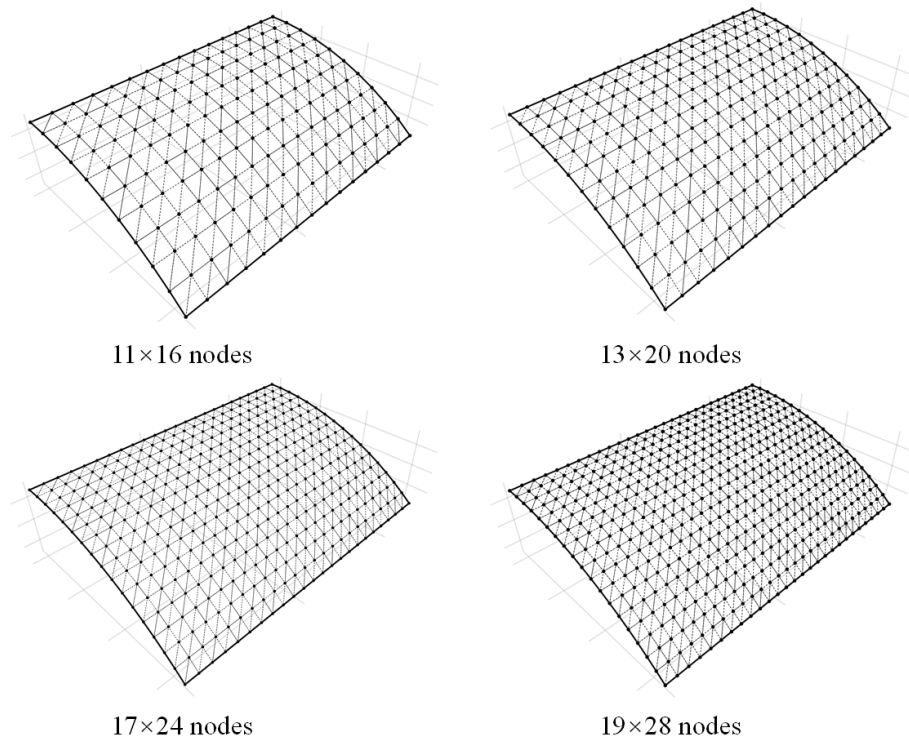


Figure 6: Meshfree discretizations for Scordelis-Lo roof problem.

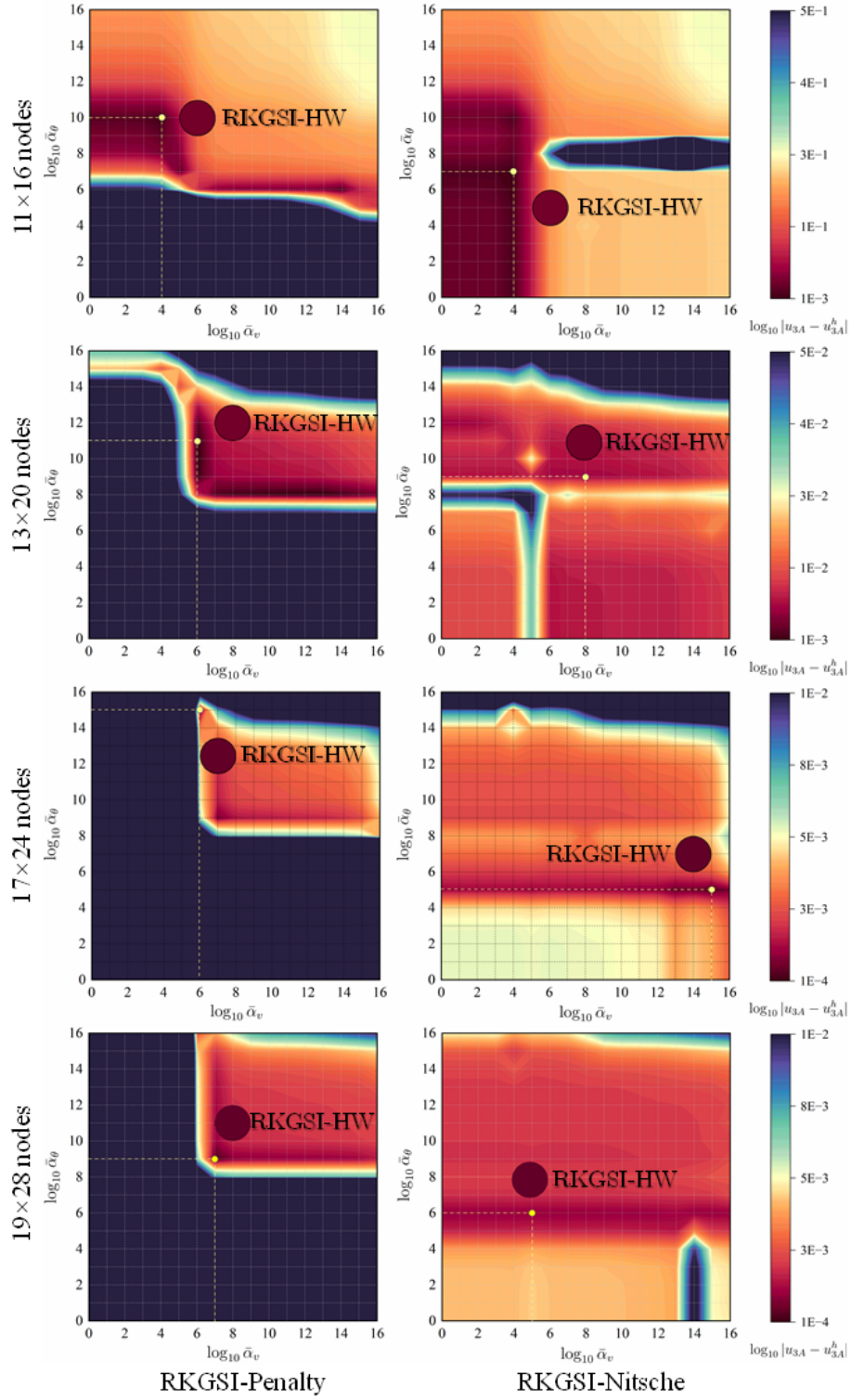


Figure 7: Sensitivity comparison of α_v and α_θ for Scordelis-Lo problem.

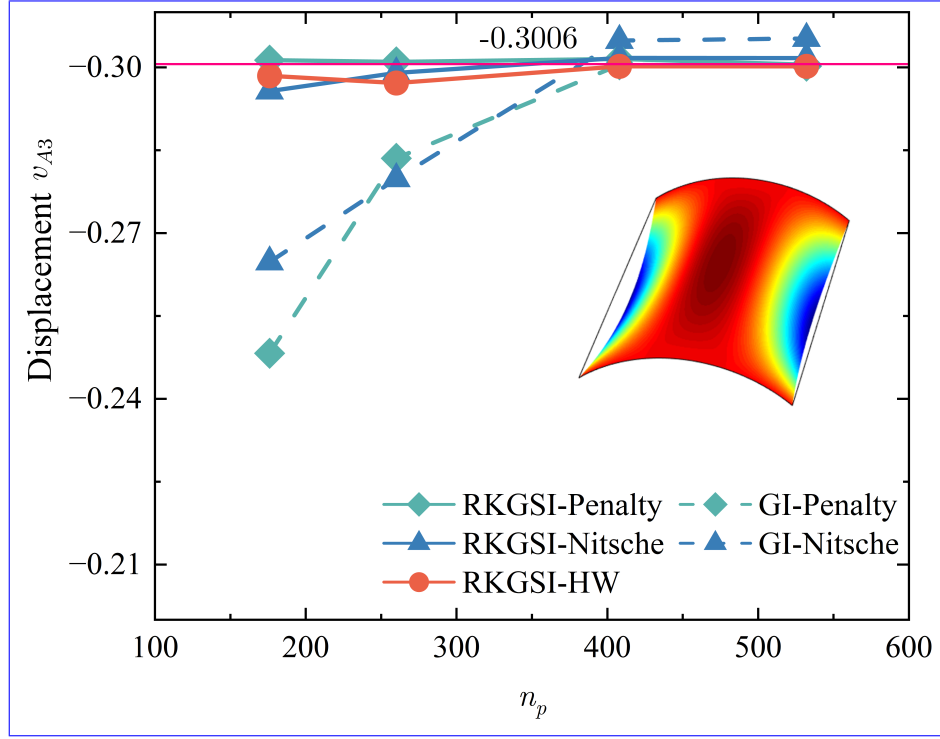


Figure 8: Displacement convergence for Scordelis-Lo roof problem.

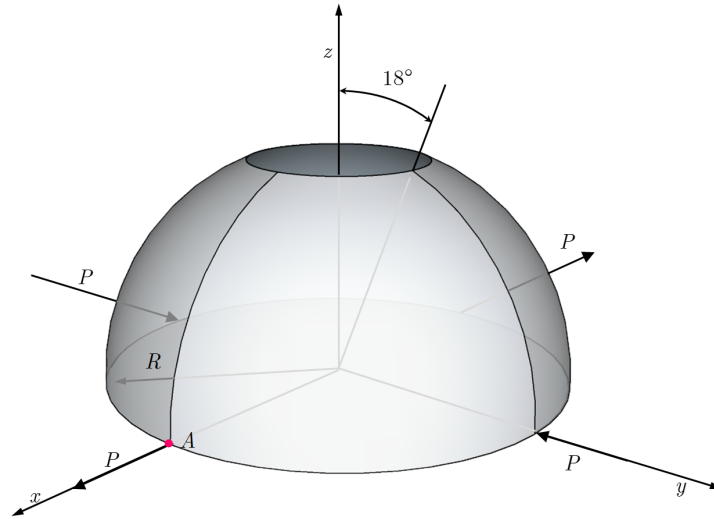
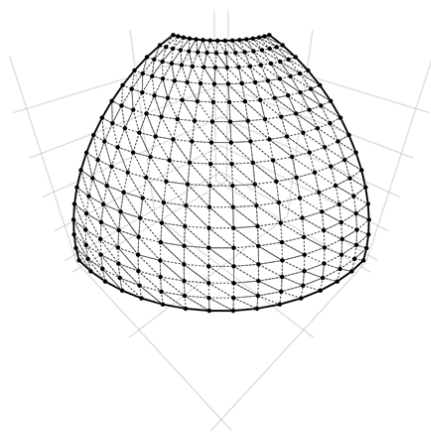
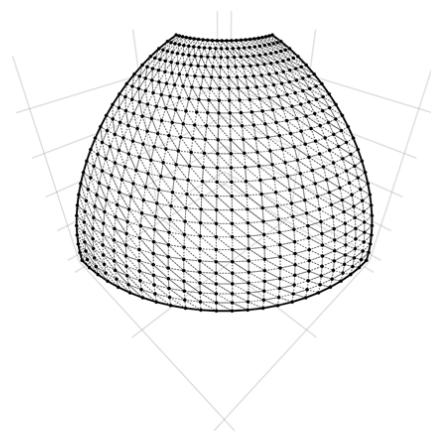


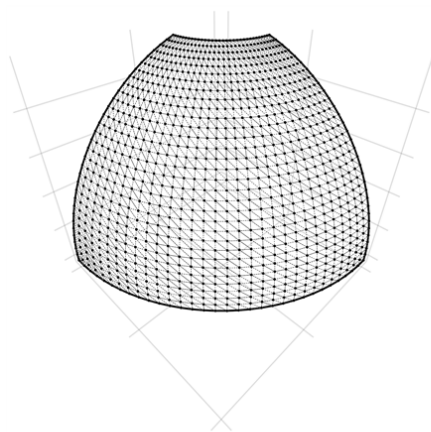
Figure 9: Description of pinched hemispherical shell problem.



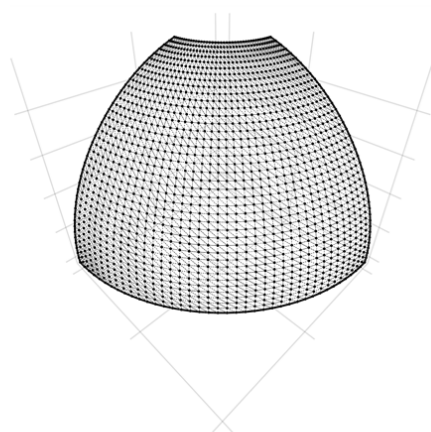
16×16 nodes



24×24 nodes



32×32 nodes



40×40 nodes

Figure 10: Meshfree discretizations for pinched hemispherical shell problem.

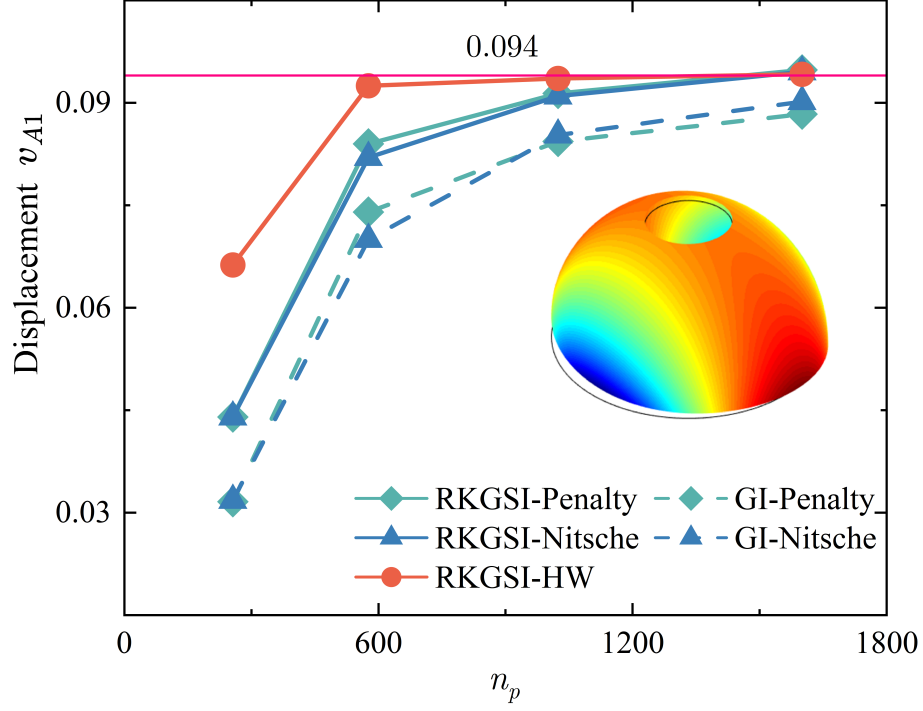


Figure 11: Displacement convergence for pinched hemispherical shell problem.

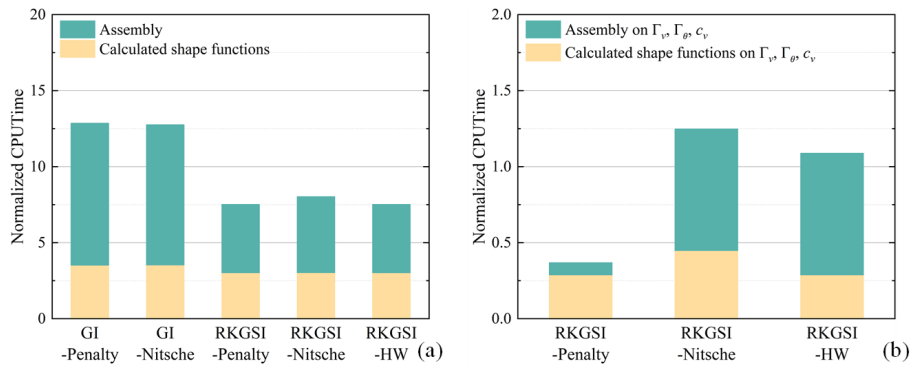


Figure 12: Efficiency comparison for pinched hemispherical shell problem: (a) Whole domain; (b) Essential boundaries

435 6. Conclusion

436 In this study, an efficient and quasi-consistent meshfree thin shell formu-
437 lation was presented to naturally enforce the essential boundary conditions.
438 Mixed formulation with the Hu-Washizu principle weak form is adopted, where
439 the traditional meshfree shape functions discretized the displacement, and the
440 strains and stresses were expressed by the reproducing kernel smoothed gradi-
441 ents and the covariant bases, respectively. The smoothed gradient naturally
442 embedded the first second-order integration constraints and has a quasi varia-
443 tional consistency for the curved models in each integration cell. Owing to the
444 Hu-Washizu variational principle, the essential boundary condition enforcement
445 has a similar form with the conventional Nitsche’s method; both have consistent
446 and stabilized terms. The costly high order derivatives in the Nitsche’s consis-
447 tent term have been replaced by the smoothed gradients, which improved the
448 computational speed due to the reproducing kernel gradient smoothing frame-
449 work. Furthermore, the stabilized term naturally existed in the Hu-Washizu
450 weak form, and the artificial parameter needed in Nitsche’s stabilized term has
451 vanished, which can automatically maintain the coercivity for the stiffness ma-
452 trix. Based on general reproducing kernel gradient smoothing framework, the
453 proposed methodology can be trivially extended to high order basis meshfree for-
454 mulation. The numerical results demonstrated that the proposed Hu-Washizu
455 quasi-consistent meshfree thin shell formulation showed excellent accuracy, ef-
456 ficiency, and stability.

Acknowledgment

The support of this work by the National Natural Science Foundation of China (12102138, 52350410467) and the Natural Science Foundation of Fujian Province of China (2023J01108, 2022J05056) is gratefully acknowledged.

461 Appendix A. Green's theorems for in-plane vector

462 This Appendix discusses two kinds of Green's theorems used for the devel-
 463 opment of the proposed meshfree method. For an arbitrary vectors v^α and a
 464 scalar function f , with Green's theorem for in-plane vector, the first Green's
 465 theorem is listed as follows [39]:

$$\begin{aligned} \int_{\Omega} f_{,\alpha} v^\alpha d\Omega &= \int_{\Gamma} f v^\alpha n_\alpha d\Gamma - \int_{\Omega} f (v_{,\alpha}^\alpha + \Gamma_{\beta\alpha}^\beta v^\alpha) d\Omega \\ &= \int_{\Gamma} f v^\alpha n_\alpha d\Gamma - \int_{\Omega} f v^\alpha|_\alpha d\Omega \end{aligned} \quad (\text{A.1})$$

466 where $\Gamma_{\alpha\beta}^\gamma = \mathbf{a}_{\alpha,\beta} \cdot \mathbf{a}^\gamma$ denotes the Christoffel symbol of the second kind. $v^\alpha|_\alpha$
 467 can be represented as the in-plane covariant derivative of the vector v^α :

$$v^\alpha|_\alpha = v_{,\alpha}^\alpha + \Gamma_{\beta\alpha}^\beta v^\alpha \quad (\text{A.2})$$

468 The second Green's theorem is established with a mixed form of second
 469 order derivative. Let $A^{\alpha\beta}$ can be an arbitrary symmetric second order tensor,
 470 the Green's theorem yields [39]:

$$\begin{aligned} \int_{\Omega} f_{,\alpha}|_\beta A^{\alpha\beta} d\Omega &= \int_{\Gamma} f_{,\gamma} n^\gamma A^{\alpha\beta} n_\alpha n_\beta d\Gamma - \int_{\Gamma} f (A^{\alpha\beta} s_\alpha n_\beta)_{,\gamma} s^\gamma d\Gamma + [[f A^{\alpha\beta} s_\alpha n_\beta]]_{\mathbf{x} \in C} \\ &\quad - \int_{\Gamma} f (A_{,\beta}^{\alpha\beta} n_\alpha + \Gamma_{\alpha\beta}^\gamma A^{\alpha\beta} n_\gamma + \Gamma_{\gamma\beta}^\gamma A^{\alpha\beta} n_\alpha) d\Gamma \\ &\quad + \int_{\Omega} f \left(\Gamma_{\alpha\beta,\gamma}^\gamma A^{\alpha\beta} + \Gamma_{\alpha\beta}^\gamma A_{,\gamma}^{\alpha\beta} + \Gamma_{\eta\gamma}^\eta \Gamma_{\alpha\beta}^\gamma A^{\alpha\beta} \right. \\ &\quad \left. + A_{,\alpha\beta}^{\alpha\beta} + \Gamma_{\gamma\beta,\alpha}^\gamma A^{\alpha\beta} + 2\Gamma_{\gamma\alpha}^\gamma A_{,\beta}^{\alpha\beta} + \Gamma_{\gamma\alpha}^\gamma \Gamma_{\eta\beta}^\eta A^{\alpha\beta} \right) d\Omega \\ &= \int_{\Gamma} f_{,\gamma} n^\gamma A^{\alpha\beta} n_\alpha n_\beta d\Gamma - \int_{\Gamma} f (A^{\alpha\beta} s_\alpha n_\beta)_{,\gamma} s^\gamma d\Gamma + [[f A^{\alpha\beta} s_\alpha n_\beta]]_{\mathbf{x} \in C} \\ &\quad - \int_{\Gamma} f A^{\alpha\beta}|_\beta n_\alpha d\Gamma + \int_{\Omega} f A^{\alpha\beta}|_{\alpha\beta} d\Omega \end{aligned} \quad (\text{A.3})$$

471 with

$$A^{\alpha\beta}|_\beta = A_{,\beta}^{\alpha\beta} + \Gamma_{\beta\gamma}^\alpha A^{\beta\gamma} + \Gamma_{\gamma\beta}^\gamma A^{\alpha\beta} \quad (\text{A.4})$$

472

$$\begin{aligned} A^{\alpha\beta}|_{\alpha\beta} &= \Gamma_{\alpha\beta,\gamma}^\gamma A^{\alpha\beta} + \Gamma_{\alpha\beta}^\gamma A_{,\gamma}^{\alpha\beta} + \Gamma_{\eta\gamma}^\eta \Gamma_{\alpha\beta}^\gamma A^{\alpha\beta} \\ &\quad + A_{,\alpha\beta}^{\alpha\beta} + \Gamma_{\gamma\beta,\alpha}^\gamma A^{\alpha\beta} + 2\Gamma_{\gamma\alpha}^\gamma A_{,\beta}^{\alpha\beta} + \Gamma_{\gamma\alpha}^\gamma \Gamma_{\eta\beta}^\eta A^{\alpha\beta} \end{aligned} \quad (\text{A.5})$$

473 For the sake of brevity, the notion of covariant derivative is extended to a
 474 scalar function as:

$$f|_\alpha = f_{,\alpha} + \Gamma_{\beta\alpha}^\beta f \quad (\text{A.6})$$

475

$$f|_\beta n_\alpha = f_{,\beta} n_\alpha + \Gamma_{\alpha\beta}^\gamma f n_\gamma + \Gamma_{\gamma\beta}^\gamma f n_\alpha \quad (\text{A.7})$$

476

$$\begin{aligned} f|_{\alpha\beta} &= \Gamma_{\alpha\beta,\gamma}^\gamma f + \Gamma_{\alpha\beta}^\gamma f_{,\gamma} + \Gamma_{\eta\gamma}^\eta \Gamma_{\alpha\beta}^\gamma f \\ &\quad + f_{,\alpha\beta} + \Gamma_{\gamma\beta,\alpha}^\gamma f + 2\Gamma_{\gamma\alpha}^\gamma f_{,\beta} + \Gamma_{\gamma\alpha}^\gamma \Gamma_{\eta\beta}^\eta f \end{aligned} \quad (\text{A.8})$$

477 Appendix B. Derivations for stiffness metrics and force vectors

478 This Appendix details the derivations of stiffness matrices and force vectors
 479 in Eqs. (53)-(55), where the relationships of Eqs. (40), (41), (44) and (46) are
 480 used herein. Firstly, the membrane strain terms are considered as follows:

$$\begin{aligned}
 & \sum_{C=1}^{n_e} \int_{\Omega_C} \delta \tilde{\varepsilon}_{\alpha\beta}^h h C^{\alpha\beta\gamma\eta} \tilde{\varepsilon}_{\gamma\eta}^h d\Omega \\
 &= \sum_{C=1}^{n_e} \sum_{I,J=1}^{n_p} \delta \mathbf{d}_I \cdot \underbrace{\int_{\Omega_C} \tilde{\varepsilon}_{\alpha\beta I} h C^{\alpha\beta\gamma\eta} \mathbf{a}_\gamma \mathbf{q}^T d\Omega \mathbf{G}^{-1} \bar{\mathbf{g}}_{\eta J}}_{\tilde{\mathbf{g}}_I^{\eta T}} \cdot \mathbf{d}_J \\
 &= \sum_{C=1}^{n_e} \sum_{I,J=1}^{n_p} \delta \mathbf{d}_I \cdot \int_{\Gamma_C \cap \Gamma_v} \Psi_J \mathbf{q}^T \underbrace{\mathbf{G}^{-1} \tilde{\mathbf{g}}_I^\alpha n_\alpha}_{\tilde{\mathbf{T}}_{NI}} d\Gamma \cdot \mathbf{d}_J \\
 &= \sum_{I,J=1}^{n_p} \delta \mathbf{d}_I \cdot \int_{\Gamma_v} \tilde{\mathbf{T}}_{NI} \Psi_J d\Gamma \cdot \mathbf{d}_J
 \end{aligned} \tag{B.1}$$

481 with

$$482 \quad \tilde{\mathbf{g}}_I^\alpha = \mathbf{q} \mathbf{a}_\beta h C^{\alpha\beta\gamma\eta} \tilde{\varepsilon}_{\gamma\eta I} \tag{B.2}$$

$$483 \quad \tilde{\mathbf{T}}_{NI} = \mathbf{q}^T \mathbf{G}^{-1} \tilde{\mathbf{g}}_I^\alpha n_\alpha \tag{B.3}$$

Following this path, the bending strain terms can be reorganized by:

$$\begin{aligned}
 & \sum_{C=1}^{n_e} \int_{\Omega_C} \delta \tilde{\kappa}_{\alpha\beta}^h \frac{h^3}{12} C^{\alpha\beta\gamma\eta} \tilde{\kappa}_{\gamma\eta}^h d\Omega \\
 &= \sum_{C=1}^{n_e} \sum_{I,J=1}^{n_p} \delta \mathbf{d}_I \cdot \underbrace{\int_{\Omega_C} \tilde{\kappa}_{\alpha\beta I} \frac{h^3}{12} C^{\alpha\beta\gamma\eta} \mathbf{a}_3 \mathbf{q}^T d\Omega \mathbf{G}^{-1} \bar{\mathbf{g}}_{\gamma\eta J}}_{\tilde{\mathbf{g}}_I^{\gamma\eta T}} \cdot \mathbf{d}_J \\
 &= \sum_{C=1}^{n_e} \sum_{I,J=1}^{n_p} \delta \mathbf{d}_I \cdot \left(\begin{aligned} & \int_{\Gamma_C \cap \Gamma_\theta} \underbrace{\mathbf{q}^T \mathbf{G}^{-1} \tilde{\mathbf{g}}_I^{\alpha\beta} n_\alpha n_\beta}_{\tilde{\mathbf{M}}_{nnI}} n^\gamma \Psi_{J,\gamma} d\Gamma \\ & - \int_{\Gamma_C \cap \Gamma_v} \underbrace{(\mathbf{q}_{|\beta}^T \mathbf{G}^{-1} \tilde{\mathbf{g}}_I^{\alpha\beta} n_\alpha + (\mathbf{q}^T \mathbf{G}^{-1} \tilde{\mathbf{g}}_I^{\alpha\beta} s_\alpha n_\beta)_{,\gamma} s^\gamma)}_{\tilde{\mathbf{T}}_{MI}} \Psi_J d\Gamma \\ & + [[\underbrace{\mathbf{q}^T \mathbf{G}^{-1} \tilde{\mathbf{g}}_I^{\alpha\beta} s_\alpha n_\beta}_{\tilde{\mathbf{P}}_I \mathbf{a}_3} \Psi_J]]_{\mathbf{x} \in C_C \cap C_v} \end{aligned} \right) \cdot \mathbf{d}_J \\
 &= \sum_{I,J=1}^{n_p} \delta \mathbf{d}_I \cdot \left(\int_{\Gamma_\theta} \tilde{\mathbf{M}}_{nnI} n^\gamma \Psi_{J,\gamma} d\Gamma - \int_{\Gamma_v} \tilde{\mathbf{T}}_{MI} \Psi_J d\Gamma + [[\tilde{\mathbf{P}}_I \Psi_J]]_{\mathbf{x} \in C_v} \right)
 \end{aligned} \tag{B.4}$$

484 with

$$\tilde{\mathbf{g}}_I^{\alpha\beta} = \int_{\Omega_C} \mathbf{q} \frac{h^3}{12} C^{\alpha\beta\gamma\eta} \mathbf{a}_3 \tilde{\kappa}_{\gamma\eta I} d\Omega \quad (\text{B.5})$$

485

$$\begin{cases} \tilde{M}_{nnI} = \mathbf{q}^T \mathbf{G}^{-1} \tilde{\mathbf{g}}_I^{\alpha\beta} n_\alpha n_\beta \\ \tilde{\mathbf{T}}_{MI} = \mathbf{q}_{|\beta}^T \mathbf{G}^{-1} \tilde{\mathbf{g}}_I^{\alpha\beta} n_\alpha + (\mathbf{q}^T \mathbf{G}^{-1} \tilde{\mathbf{g}}_I^{\alpha\beta} s_\alpha n_\beta)_{,\gamma} s^\gamma \\ \tilde{\mathbf{P}}_I = \mathbf{q}^T \mathbf{G}^{-1} \tilde{\mathbf{g}}_I^{\alpha\beta} s_\alpha n_\beta \cdot \mathbf{a}_3 \end{cases} \quad (\text{B.6})$$

References

- [1] L. H. Donnell, Beams, Plates and Shells, McGraw-Hill, 1976.
- [2] [S. Ahmad, B. M. Irons, O. C. Zienkiewicz, Analysis of thick and thin shell structures by curved finite elements, International Journal for Numerical Methods in Engineering 2 \(1970\) 419–451.](#)
- [3] T. J. Hughes, The Finite Element Method: Linear Static and Dynamic Finite Element Analysis, Dover Publications, Mineola, New York, 2000.
~~T. Belytschko, Y. Y. Lu, L. Gu, Element-free Galerkin methods, International Journal for Numerical Methods in Engineering 37 (1994) 229–256.~~
- [4] [J. C. Simo, D. D. Fox, On a stress resultant geometrically exact shell model. Part I: Formulation and optimal parametrization, Computer Methods in Applied Mechanics and Engineering 72 \(1989\) 267–304.](#)
~~W. K. Liu, S. Jun, Y. F. Zhang, Reproducing kernel particle methods, International Journal for Numerical Methods in Fluids 20 (1995) 1081–1106.~~
- [5] [P. Krysl, T. Belytschko, Analysis of thin shells by the Element-Free Galerkin method, International Journal of Solids and Structures 33 \(1996\) 3057–3080.](#)
- [6] [D. Millán, A. Rosolen, M. Arroyo, Thin shell analysis from scattered points with maximum-entropy approximants, International Journal for Numerical Methods in Engineering 85 \(2011\) 723–751.](#)
~~J. S. Chen, M. Hillman, S. W. Chi, Meshfree methods: Progress made after 20 Years, Journal of Engineering Mechanics 143 (2017) 04017001.~~
- [7] [D. Wang, C. Song, H. Peng, A circumferentially enhanced Hermite reproducing kernel meshfree method for buckling analysis of Kirchhoff–Love cylindrical shells, International Journal of Structural Stability and Dynamics 15 \(2015\) 1450090.](#)
~~P. Krysl, T. Belytschko, Analysis of thin shells by the Element-Free Galerkin method, International Journal of Solids and Structures 33 (1996) 3057–3080.~~
- [8] [M. Behzadinasab, M. Alaydin, N. Trask, Y. Bazilevs, A general-purpose, inelastic, rotation-free Kirchhoff–Love shell formulation for peridynamics, Computer Methods in Applied Mechanics and Engineering 389 \(2022\) 114422.](#)
- [9] [J. Kiendl, K. U. Bletzinger, J. Linhard, R. Wüchner, Isogeometric shell analysis with Kirchhoff–Love elements, Computer Methods in Applied Mechanics and Engineering 198 \(2009\) 3902–3914.](#)
- [10] G. R. Liu, Meshfree Methods: Moving Beyond the Finite Element Method, Second Edition, Crc Press, 2009.

- [11] ~~X. Zhang, K. Z. Song, M. W. Lu, X. Liu, Meshless methods based on collocation with radial basis functions, Computational Mechanics 26 (2000) 333–343.~~
- [12] ~~J. S. Chen, M. Hillman, S. W. Chi, Meshfree methods: Progress made after 20 Years, Journal of Engineering Mechanics 143 (2017) 04017001.~~
~~D. Millán, A. Rosolen, M. Arroyo, Thin shell analysis from scattered points with maximum-entropy approximants, International Journal for Numerical Methods in Engineering 85 (2011) 723–751.~~
- [13] ~~X. Zhang, Z. Chen, Y. Liu, The Material Point Method: A Continuum-Based Particle Method for Extreme Loading Cases, Academic Press, Oxford, 2017.~~
- [14] ~~P. Suchde, T. Jacquemin, O. Davydov, Point Cloud Generation for Meshfree Methods: An Overview, Archives of Computational Methods in Engineering 30 (2022) 889–915.~~
- [15] ~~L. Wang, M. Hu, Z. Zhong, F. Yang, Stabilized Lagrange Interpolation Collocation Method: A meshfree method incorporating the advantages of finite element method, Computer Methods in Applied Mechanics and Engineering 404 (2023) 115780.~~
~~P. Suchde, T. Jacquemin, O. Davydov, Point Cloud Generation for Meshfree Methods: An Overview, Archives of Computational Methods in Engineering 30 (2022) 889–915.~~
- [16] L. Deng, D. Wang, An accuracy analysis framework for meshfree collocation methods with particular emphasis on boundary effects, Computer Methods in Applied Mechanics and Engineering 404 (2023) 115782.
- [17] J. Wang, M. Hillman, Upwind reproducing kernel collocation method for convection-dominated problems, Computer Methods in Applied Mechanics and Engineering 420 (2024) 116711.
- [18] ~~J. Wang, M. Behzadinasab, W. Li, Y. Bazilevs, A stable formulation of correspondence-based peridynamics with a computational structure of a method using nodal integration, International Journal for Numerical Methods in Engineering (2024) e7465.~~
- [19] ~~T. Belytschko, Y. Y. Lu, L. Gu, Element-free Galerkin methods, International Journal for Numerical Methods in Engineering 37 (1994) 229–256.~~
- [20] ~~W. K. Liu, S. Jun, Y. F. Zhang, Reproducing kernel particle methods, International Journal for Numerical Methods in Fluids 20 (1995) 1081–1106.~~
- [21] S. Fernández-Méndez, A. Huerta, Imposing essential boundary conditions in mesh-free methods, Computer Methods in Applied Mechanics and Engineering 193 (2004) 1257–1275.

- [22] X. Li, Error estimates for the moving least-square approximation and the element-free Galerkin method in n-dimensional spaces, *Applied Numerical Mathematics* 99 (2016) 77–97.
- [23] J. Wu, D. Wang, An accuracy analysis of Galerkin meshfree methods accounting for numerical integration, *Computer Methods in Applied Mechanics and Engineering* 375 (2021) 113631.
- [24] J. S. Chen, H. P. Wang, New boundary condition treatments in meshfree computation of contact problems, *Computer Methods in Applied Mechanics and Engineering* 187 (2000) 441–468.
- [25] D. Liu, Y. M. Cheng, The interpolating element-free Galerkin (IEFG) method for three-dimensional potential problems, *Engineering Analysis with Boundary Elements* 108 (2019) 115–123.
- [26] V. Ivannikov, C. Tiago, P. M. Pimenta, On the boundary conditions of the geometrically nonlinear Kirchhoff–Love shell theory, *International Journal of Solids and Structures* 51 (2014) 3101–3112.
- [27] Y. Y. Lu, T. Belytschko, L. Gu, A new implementation of the element free Galerkin method, *Computer Methods in Applied Mechanics and Engineering* 113 (1994) 397–414.
- [28] T. Zhu, S. N. Atluri, A modified collocation method and a penalty formulation for enforcing the essential boundary conditions in the element free Galerkin method, *Computational Mechanics* 21 (1998) 211–222.
- [29] S. Skatulla, C. Sansour, Essential boundary conditions in meshfree methods via a modified variational principle: Applications to shell computations, *Computer Assisted Mechanics and Engineering Sciences* 15 (2008) 123–142.
- [30] [Y. Guo, Z. Zou, M. Ruess, Isogeometric multi-patch analyses for mixed thin shells in the framework of non-linear elasticity, Computer Methods in Applied Mechanics and Engineering 380 \(2021\) 113771.](#)
- [31] [J. Wang, G. Zhou, M. Hillman, A. Madra, Y. Bazilevs, J. Du, K. Su, Consistent immersed volumetric Nitsche methods for composite analysis, Computer Methods in Applied Mechanics and Engineering 385 \(2021\) 114042.](#)
- [32] J. S. Chen, C. T. Wu, S. Yoon, Y. You, A stabilized conforming nodal integration for Galerkin mesh-free methods, *International Journal for Numerical Methods in Engineering* 50 (2001) 435–466.
- [33] J. S. Chen, M. Hillman, M. Rüter, An arbitrary order variationally consistent integration for Galerkin meshfree methods, *International Journal for Numerical Methods in Engineering* 95 (2013) 387–418.

- 603 [34] Q. Duan, X. Li, H. Zhang, T. Belytschko, Second-order accurate derivatives
604 and integration schemes for meshfree methods, *International Journal for*
605 *Numerical Methods in Engineering* 92 (2012) 399–424.
- 606 [35] D. Wang, J. Wu, An inherently consistent reproducing kernel gradient
607 smoothing framework toward efficient Galerkin meshfree formulation with
608 explicit quadrature, *Computer Methods in Applied Mechanics and Engi-*
609 *neering* 349 (2019) 628–672.
- 610 [36] J. Wang, X. Ren, A consistent projection integration for Galerkin meshfree
611 methods, *Computer Methods in Applied Mechanics and Engineering* 414
612 (2023) 116143.
- 613 [37] J. Wu, X. Wu, Y. Zhao, D. Wang, A consistent and efficient method for
614 imposing meshfree essential boundary conditions via hellinger-reissner vari-
615 ational principle., *Chinese Journal of Theoretical and Applied Mechanics*
616 54 (2022) 3283–3296.
- 617 [38] J. Wu, X. Wu, Y. Zhao, D. Wang, A rotation-free Hellinger-Reissner mesh-
618 free thin plate formulation naturally accommodating essential boundary
619 conditions, *Engineering Analysis with Boundary Elements* 154 (2023) 122–
620 140.
- 621 [39] J. Benzaken, J. A. Evans, S. F. McCormick, R. Tamstorf, Nitsche’s method
622 for linear Kirchhoff–Love shells: Formulation, error analysis, and verifica-
623 tion, *Computer Methods in Applied Mechanics and Engineering* 374 (2021)
624 113544.
- 625 [40] H. Dah-wei, A method for establishing generalized variational principle,
626 *Applied Mathematics and Mechanics* 6 (1985) 501–509.
- 627 [41] H. Du, J. Wu, D. Wang, J. Chen, A unified reproducing kernel gradient
628 smoothing Galerkin meshfree approach to strain gradient elasticity, *Com-*
629 *putational Mechanics* 70 (2022) 73–100.
630 ~~J. Kiendl, K. U. Bletzinger, J. Linhard, R. Wüchner, Isogeometric shell~~
631 ~~analysis with Kirchhoff–Love elements, *Computer Methods in Applied*~~
632 ~~*Mechanics and Engineering* 198 (2009) 3902–3914.~~
- 633 [42] R. H. Macneal, R. L. Harder, A proposed standard set of problems to test
634 finite element accuracy, *Finite Elements in Analysis and Design* 1 (1985)
635 3–20.